TRANSITION METAL COMPLEXES OF N,N-BIS(DIALKYLPHOSPHINOMETHYL)AMINOMETHANE DERIVATIVES: A DFT STUDY

by

Ahmet Köseoğlu

B.S., Chemistry, Boğaziçi University, 2005

Submitted to the Institute for Graduate Studies in
Science and Engineering in partial fulfillment of
the requirements for the degree of
Master of Science

Graduate Program in Chemistry
Boğaziçi University

2007

TRANSITION METAL COMPLEXES OF
N,N-(BISDIALKYLPHOSPHINOMETHYL)AMINOMETHANE) DERIVATIVES:
A DFT STUDY

APPROVED BY:

Prof. Tereza Varnalı . . . . . .
(Thesis Supervisor)

Prof. Viktorya Aviyente . . . . . .

Prof. Türkan Haliloğlu . . . . . .

DATE OF APPROVAL: 06.06.2007

ACKNOWLEDGEMENT

I would like to express my gratitude to my thesis supervisor, Prof.Dr. Tereza Varnalı for her support and guidence throughout this work. I would also like to mention her encouragement and patience, giving me inspiration and hope when I was stuck.

I also would like to thank to Prof. Dr. Viktorya Aviyente and Prof. Dr. Türkan Haliloğlu for their advices and comments on the final manuscripts.

I would like to thank all the members of the chemistry department especially to Hülya Metiner, always willing to help and share the problems.

Finally, I would like to express my indebtedness to my family for their continuous support throughout my life.

This work has been supported B.Ü. Research Funds Project No: 06B507

ABSTRACT

TRANSITION METAL COMPLEXES OF N,N-BIS(DIALKYLPHOSPHINOMETHYL) AMINOMETHANE DERIVATIVES: A DFT STUDY

Aminomethylphosphine complexes are used as catalysts in various organic reactions which involve heterogeneous and homogenous processes. Some examples in which aminomethylphosphine complexes are used as catalysts are hydrogenation reactions, hydroformylation reactions and Heck reactions. Some of these studies involve attempts to obtain asymmetric catalysis by making chiral complexes and some involve aminomethylphosphine complexes attached to a solid support in which modifications on the aminomethylphosphine complexes were done. The effect of these modifications, if any, on the structure of the aminomethylphosphine complexes may play an important role for both their reactivities and selectivities. Though papers of experimental studies on these complexes exist in the literature, we have not encountered a computational study. The aim of this study is to understand the effect of different R groups and find a trend for different metal and/or halogen complexes if any.

In this work, various transition metal complexes of aminomethylphosphines have been studied by using DFT method. A systematic approach altering the metal M, the halogen X and the substituent R on the phosphorus atom was taken. The transition metals Ni, Pd, Pt which lie on the same group on the periodic table and Rh, which lies on the same period with Pd have been used for complexation. The R groups on the phosphorous atoms utilized are methyl, cyclohexyl and phenyl groups. The halogens Cl, Br and I were used as the coligands. Electronic and structural properties of each complex have been examined. It was found that, phenyl group, which is capable of making π-bonding with P and N atoms by resonance, has significant electron withdrawing effect, that halogen atoms with varying electronegativities and metal centers with different electronegativities and sizes also affect the structure of the complex and the charge distribution on it.

ÖZET

N,N-BİS(DiALKiLFOSFİNOMETiL) AMİNOMETAN TÜREVLERİ GEÇİŞ METAL COMPLEKSLERİ: DFT ÇALIŞMASI

Aminometilfosfin kompleksleri heterojen ve homojen işlemler içeren çeşitli organik reaksiyonlarda katalizör olarak kullanılmaktadırlar. Aminometilfosfin komplekslerinin katalizör olarak kullanıldığı reaksiyonlara örnek olarak hidrojenleme, hidroformülleme ve Heck reaksiyonları örnek olarak gösterilebilir. Bu çalışmalardan bazılarında kiral aminometilfofin kompleksleri modifiye edilerek asimetrik sentez yapılmaya çalışılmış ve bazılarında da katı desteğe dayalı fosfinler kullanılmıştır. Bu modifikasyonların aminmetilfosfin komplekslerinin yapıları üzerinde etkileri, eğer varsa, seçicilikleri ve reaktiflikleri üzerinde önemli rol oynayabilirler. Literatürde bu kompleksler üzerinde deneysel çalışma olmasına rağmen, hesapsal bir çalışmaya rastlanmamıştır. Bu çalışmanın amacı farklı R guplarının etkilerini incelemek ve eğer varsa farklı metal ve / veya halojen kompleksleri üzerinde belirli değişimleri bulmaktır.

Bu çalışmada, DFT metodu kullanılarak çeşitli aminometilfosfin geçiş metali kompleksleri incelenmiştir. Metal M, halojen X ve fosfor P atomları üzerindeki alkil R grupları değiştirilerek sistematik bir yaklaşım uygulanmıştır. Aynı periyodda yer Ni, Pd ve Pt alan geçiş metalleri ve Pd ile aynı grupta yer alan Rh metali kompleksleşme için kullanılmıştır. Fosfor atomları üzerindeki R gruları metil, fenil ve siklohegzil olarak alınmıştır. Cl, Br ve I halojenleri koligand olarak kullanılmıştır.Elektronik ve yapısal özellikler incelenmiştir. Sonuç olarak rezonans yolu ile P ve N atomlarıyla π-bağı yapabilen fenil grubunun önemli bir elektron çekme etkisine sahip olduğu, çeşitli elektronegativite değerlerine sahip halojen atomlarının ve yine çeşitli elektronegativite değerlerine ve yarıçaplarına sahip metallerin komplekslerin geometrk yapılarını ve yük dağılımlarını önemli ölçüde etkiledikleri saptanmıştır.

TABLE OF CONTENTS

LIST OF FIGURES

LIST OF TABLES

LIST OF SYMBOLS/ ABBREVIATIONS

$E_c[\rho]$	Correlation energy
$E_x[\rho]$	Exchange energy
$J[\rho]$	Coulomb energy
$T[\rho]$	Kinetic energy of interacting electron
$T_s[\rho]$	Kinetic energy of non-interacting electron
$V_{ee}[\rho]$	Interelectronic interaction energy
V_{KS}	Kohn-Sham potential
βn	Bite angle
$v(r)$	External Potential
$v_{xc}(r)$	Exchange Correlation Potential
$\rho(r)$	Electron density
ψ_i	Kohn-Sham orbitals
Calc.	Calculated
dppm	1,2-Bis(diphenylphosphino)methane
dppe	1,2-Bis(diphenylphosphino)ethane
dppp	1,2-Bis(diphenylphosphino)propane
dppb	1,2-Bis(diphenylphosphino)butane
dppm-cyh	1,2-Bis(diphenylphosphino)cyclohexane
dppxylene	1,2-Bis(diphenylphosphino)xylene
dppm-cyb	1,2-Bis(diphenylphosphino)cyclobutane
dppm-nbr	1,2-Bis(diphenylphosphino)norbornane
Exp.	Experimental
B3LYP	Becke-3-parameter Lee-Yang-Parr
B/L	Branched over Linear
DFT	Density functional theory

DIOP	Diisooctyl phthalate
ECP	Effective core potntial
LDA	Local density Approximation
LYP	Lee-Yang-Parr correlation functional

1. INTRODUCTION

1.1. Aminomethylphosphines as Catalysts

The tertiary phosphine complexes are very important in homogenous catalysis. There are many fundamental studies of phosphine ligands [1-2]. The electronic and steric effects on the structure, bonding and catalysis have been investigated by varying the phosphine substituents [1-3].

Hoye et.al. [4] studied the hydrogenation of α-acetamidocinnamic acid in which chiral aminomethylphosphine complexes were used to obtain asymmetric catalysis but no asymmetric product was obtained. On the other hand in the hydroformylation of styrene using chiral aminomethylphosphine (Figure 1.1) complexes of platinum in the presence of $SnCl_2$, some enantioselectivity was observed with up to 31% enantiomeric excess of 2-phenylpropanol But, the yields and the reaction rates obtained from these chiral aminomethylphosphine catalysts showed no advantage over the existing catalysts.

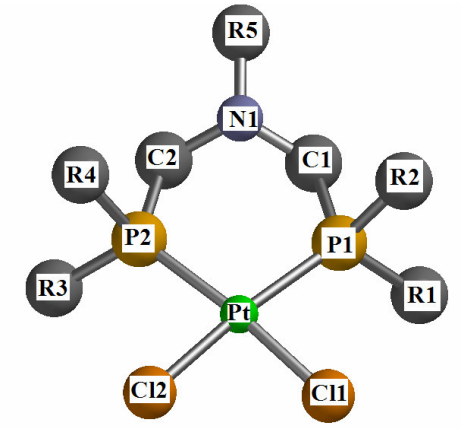

1. R1,R2,R3,R4 = Ph , R5 = CHMePh
2. R1,R2,R3,R4 = Ph , R5 = $CHMeCO_2Et$
3. R1,R2,R3,R4 = Ph , R5 = (R)-(+)-bornyl
4. R1,R2,R3,R4 = Cy , R5 = CHMePh
5. R1,R2,R3,R4 = Cy , R5 = $CHMeCO_2Et$

Figure 1.1. Chiral aminomethylphosphine catalysts used in the hydroformylation reaction of styrene

In another study [5], the transition metal aminomethylphosphine complexes were attached to the dendrimers on beads to obtain heterogenous catalysts that function as

homogenous catalysts. The Rh complexes of the G1, G2 and G3 (Figure 1.2) derivatized aminomethylphosphine ligands were used as hydroformylation catalysts (Figure 1.3).

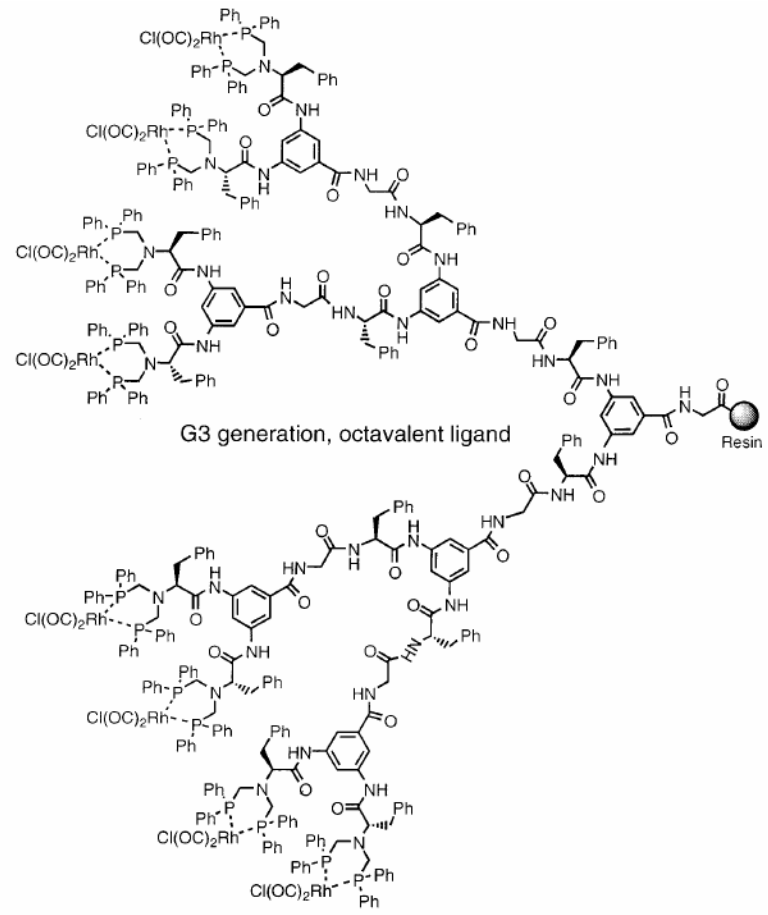

Figure 1.2. Rh complex of G3 derivatized aminomethylphosphine [5]

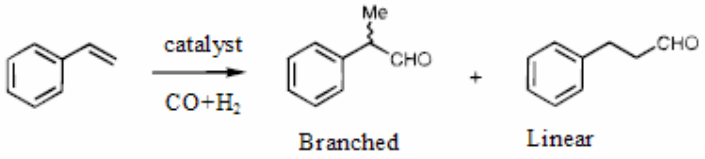

Figure 1.3. Hydroformylation of styrene in which dendrimer derivatized aminomethylphosphine catalysts were used as catalysts

These Rh complexes of dendrimer derivatized aminomethylphosphines attached on beads were found to be excellent catalysts with high conversions and high selectivity. The results are shown in Table 1.1.

Catalyst	Cycle	Time(h)	T(°C)	Conversion (%)	Branched / Linear
(G1)	1st	5	65	42	13:1
(G1)	2nd	18	65	70	12:1
(G1)	3rd	23	65	85	10:1
(G1)	4th	24	65	51	15:1
(G1)	5th	24	65	22	9:1
(G1)	6th	24	65	8	10:1
(G2)	1st	21	25	35	35:1
(G2)	1st	5	65	57	14:1
(G2)	1st	16	45	>99	16:1
(G2)	2nd	22	65	>99	11:1
(G2)	3rd	22	65	>99	12:1
(G2)	4th	22	65	>99	12:1
(G2)	5th	22	65	98	11:1
(G2)	6th	22	65	88	12:1
(G3)	1st	22	65	99	10:1
(G3)	2nd	22	65	99	9:1
(G3)	3rd	22	65	99	12:1
(G3)	4th	22	65	99	10:1
(G3)	5th	22	65	78	12:1
(G3)	6th	22	65	47	12:1

Table 1.1. The conversions and B/L ratios for dendrimer derivatized aminomethylphosphine catalysts in the hydroformylation of styrene [5]

Contrary to the general belief that polymer supported catalysts are relatively less reactive G2 catalysts are reactive up to three or more cycles.

An interesting form of supramolecular catalysis can be achieved by the combination of molecular recognition, phase transfer catalysis, and transition metal catalysis performed by one and the same catalyst in hydrogenation and C-C bond forming reactions. Reetz M.T. et .al. reported the β-cyclodextrin-modified transition metal complexes of aminomethylphosphines which function as supramolecular catalysts. These catalyses lead to high substrate selectivities when used in hydrogenations of olefins [6].

They are very active and selective when employed in the hydroformylation of olefins in a two-phase system (Figure 1.4).

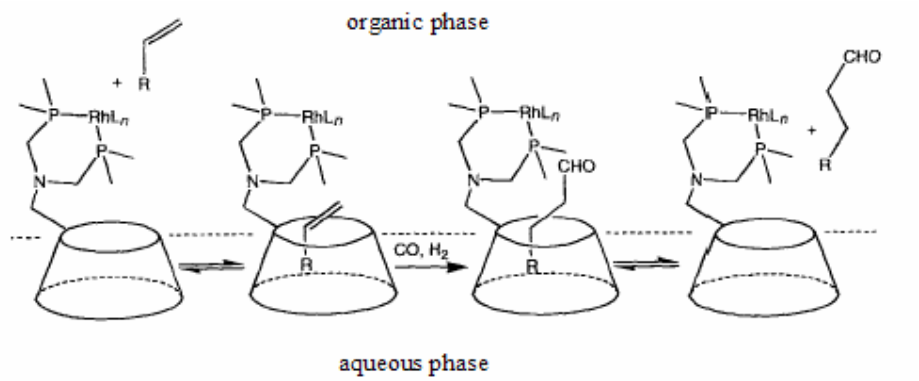

Figure 1.4. Selective phase transfer catalysis in which cyclodextrin modified Rh complexes of aminomethylphosphines were used as catalysts

1.2. Antimicrobial Activity of Aminomethylphosphines

There have been researches on the chemistry and catalytic activities of metal–phosphine complexes however, the biochemistry of aminomethylphosphines having P–C–N linkage has not been studied extensively, yet. Serindag et al synthesized novel aminomethylphosphine–metal complexes of Au(I), Ag(I), Cu(I), and Co(II) and explored some biological properties of these complexes (Figure 1.5, Figure 1.6) [7].

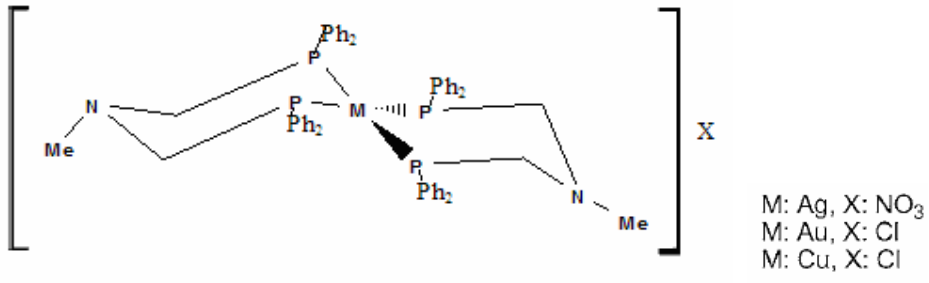

Figure 1.5. Ag, Au and Cu complexes of aminomethylsphosphines whose antimicrobial property were examined [7]

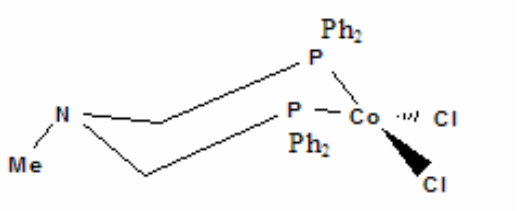

Figure 1.6. Co complex of aminomethylsphosphine whose antimicrobial property were examined [7]

Antimicrobial activities of these metal complexes were determined and it was found that the Co complex of monomer aminomethylphosphine ligand showed the best activity compared to the Au(I), Ag(I), Cu(I) complexes of dimer aminomethylphosphine ligands.

1.3. Macrocyclic, Adenine Derivatized and Water Soluble Aminomethylphosphines

The syntheses of macrocyclic polyhetero ligand systems usually require the use of high-dilution techniques that may limit their availability. Power P.P. et al showed an easy way to synthesize macrocyclic aminomethylphosphine ligands [8]. The macrocyclic ligand is shown in Figure 1.7.

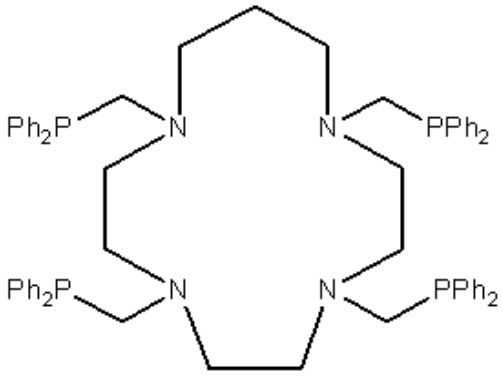

Figure 1.7. Easily synthesized macrocyclic aminomethylphosphine ligand [8]

Balueva A.S. also reported an easy way to synthesize macrocylic aminomethylphosphine complexes which has a cage structure (Figure 1.8) [9].

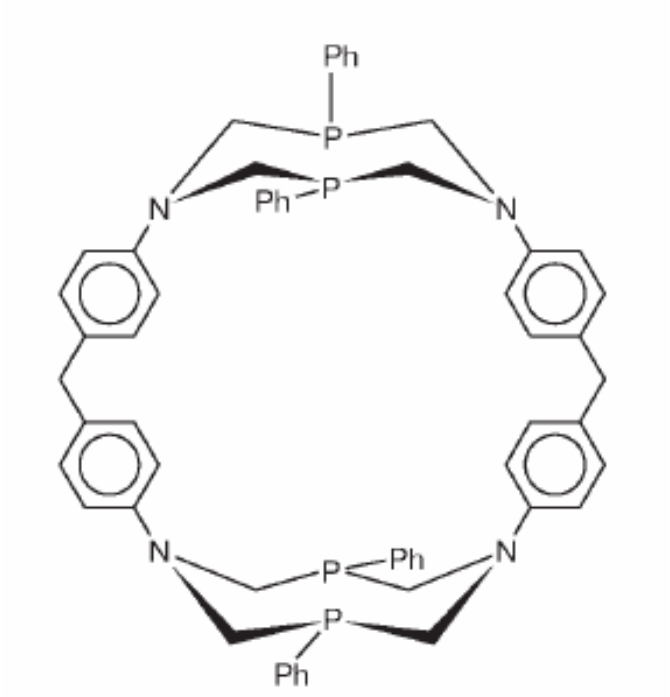

Figure 1.8. Macrocyclic aminomethylphosphine which has a cage like structure [9]

They also examined the cage property of these ligands and found out that even a water molecule cannot come inside the inner cavity.

The adenine derivatized aminomethylphosphine complexes were synthesized by an easy route which includes attachment of the aminomethylphosphine unit was into adenine through an aminodi/ trimethylene linkage at the 9-position (Figure 1.9) [10].

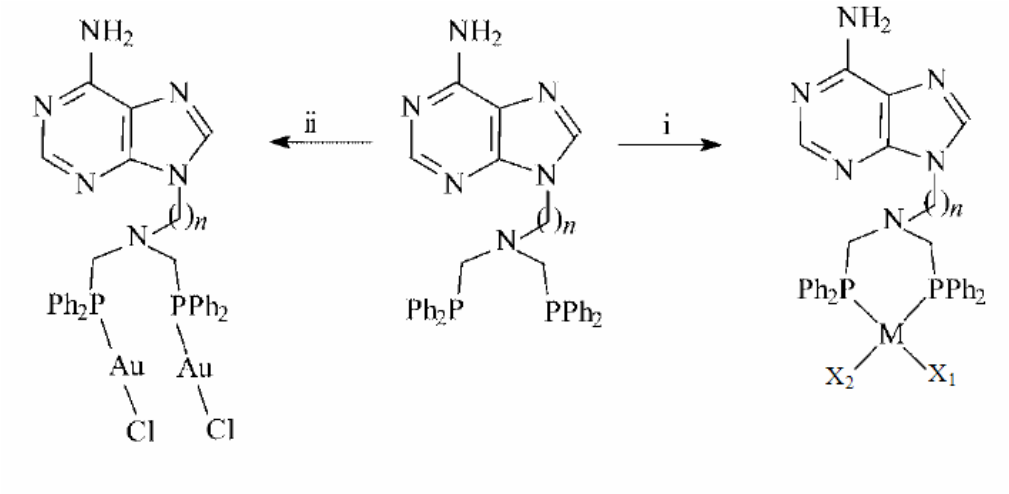

M = Pd, X_1=X_2= Cl, n=2

M = Pt, X_1=X_2= Cl, n=2

M = Pt, X_1=X_2= CH_3, n=2

M = Pt, X_1=Cl, X_2= CH_3, n=2

Figure 1.9. Adenine derivatized aminomethylphosphine complexes

The adenine derivatives prepared in this way possess two functions: they have an excellent coordination tendency toward transition metals and they can form complementary hydrogenbonding interactions. In this way enhanced biological activities are expected from these adenine derivatized amiomethylphosphine complexes and from their analogues.

Mannich-type reactions were shown to be a powerful method for the preparation of air-stable, water-soluble phosphino amino acids [11,12]. Hawkins et al reported the synthesis of some novel metalcontaining phosphino amino acids on the basis of bis(hydroxymethyl)(ferrocenylmethyl) phosphine and two water-soluble heterotrinuclear complexes of 1,5-bis(meta-dicarboxyphenyl)-3,7-bis(ferrocenylmethyl)-1,5-diaza-3,7 diphosphacyclooctane [13]. These water-soluble aminomethylphosphine complexes are shown in Figure 1.10.

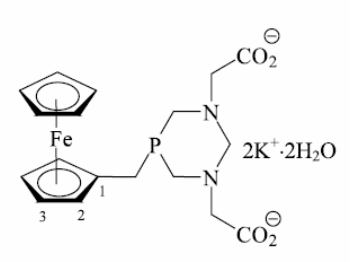

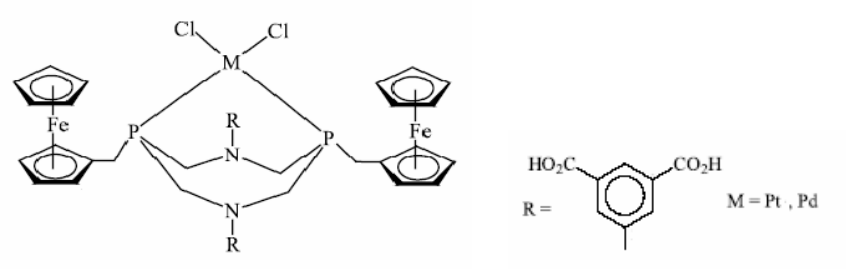

Figure 1.10. Water soluble aminomethylhosphine complexes

1.4. The Tolman Parameters and Bite angle

In 1977, Tolman reported a paper in which the steric effects of phosphorous ligands in organometallic chemistry and homogenous catalysis were discussed [14]. He showed that steric effects are extremely important to structures, spectroscopic properties, and chemical behavior of phosphorus ligands and their complexes. Increasing the size of the substituents on the phosphorous atoms will tend to result in significant changes on the M environment including an increase in the L-M-L angle, which is known as "bite angle" (Figure 1.11).

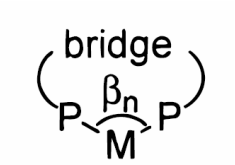

Figure 1.11. The bite angle

The Tolman parameters have been used to express ligand-property vs. catalyst-activity relationships. Bidenate ligands can prefer a specific geometry, since the bite angle is strongly dependent on the bridge between the two ligands. Metal complexes with chelating ligands which prefer a bite angle of 90^0 for instance, stabilize square planar geometries. Furthermore, ligands that enforce a well defined bite angle can be used to form

distortions of certain geometries so that destabilizing them. In this way a reaction can easily be performed by influencing the initial state, transition state or final state of the metal complex involved.

Leuveen et al studied the effect of bite angle by preparing a series of ligands forcing bite angles in the range of 100-120^0 which enable systematic studies of the effect of large bite angles on catalytic reactions [15]. They designed bidentate phosphine ligands based on xanthene-type backbones, which allowed a systematic study of bite-angle effects in transition metal catalysis. They found out that the bite angle of bidentate ligands is an important additional parameter that has a pronounced effect on rate and selectivity of metal catalyzed reactions.

In 2000 Leuveen et al reported a review about bite angle effects in metal-catalyzed C-C bond formation reactions [16]. In this review they focused on the effect of bidentate ligands which are used as catalysts in the carbon-carbon bond formation reactions. They showed that for some reactions the bite angle plays a very important role. In a 1981 paper [17] phosphine ligands with various bite angles were used to examine the effect of bite angle in the reaction of Platinum-catalyzed hydroformylation of 1-pentene (Figure 1.12).

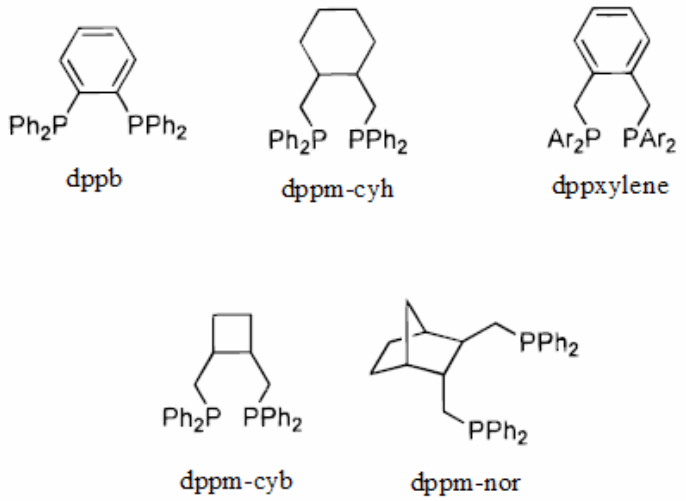

Figure 1.12. The phosphine ligands with various bite angles used in the reaction of Platinum-catalyzed hydroformylation of 1-pentene

In this study it was found that generally as the bite angle (βn) increases the rate of the reaction increases as well (Table 1.2).

ligand	βn	relative rate	linearity (%)
PPh3		100	92
dppm	72	0	90
dppe	85	10	90
dppp	91	120	71
dppb	98	400	91
dppm-cyh	90	350	90
dppxylene	90	420	91
DIOP	98	1100	96
dppm-cyb	98	1600	99
dppm-nbr	97	2100	99

Table 1.2. The relative rates of the reactions and the linearity of the products in which phosphine ligands with various bite angles were used as catalyst

The data summarized in this review show that the bite angle of bidentate ligands is an important parameter that has a significant effect on rate and selectivity of metal-catalyzed reactions.

Although the bite angle can have dramatic effects on the catalyst performance, the number of systematic studies of bite angle effects is rather limited. This is possibly due to a lack of ligands in which the bite angle can be varied in a systematic way without changing other steric and electronic properties.

1.5. Ethylene Insertion in the Metal- H Bond of $(H)M(dapam)_2^+$ Species

In a variety of catalytic processes such as polymerization reactions, hydroformylations, hydrogenations and olefin insertion reaction, the insertion of olefins into the metal-hydrogen bonds and the transformation of metal-alkyl compounds to olefins are important elementary steps [18,19]. It is generally accepted that the insertion of olefins into the Pt-H bond of cationic platinum-hydride-phosphine compounds proceeds via a four-coordinated transition state having the phosphorous ligands in a cis position and the olefin

paralel to the Pt-H bond [20-22]. The mechanism of ethylene insertion into the Pt-H bond is shown in Figure 1.13.

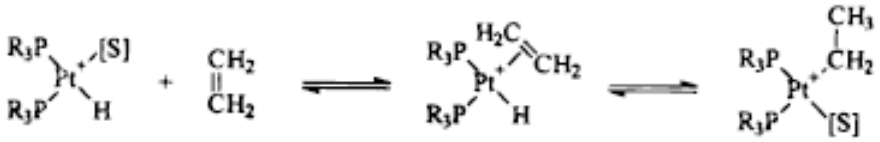

Figure 1.13. The mechanism of ethylene insertion into the Pt-H bond

Coussens and coworkers repoted Hartree-Fock, MP2, DFT and Car-Parinello type molecular dynamics simulations applied to the insertion of ethylene in cationic platinum-hydrido-diphosphine complexes [23]. The dynamics simulations on the platinum-phosphine complexes with [S] = Cl and [S] = Me showed very fast insertion of the ethylene. The small barrier calculated for the PH_3- containing complex and the fast insertion seen for the PCl_3 and PMe_3 systems suggests that the energetics of the insertion reaction are hardly affected by electron-withdrawing or electron-donating groups on the phosphorus ligands and it is concluded that as for ethylene insertion in bis(cyclopentadienyl)metallocene species and contrary to what was often the traditional point of view, this is another example of a reaction cycle for which the insertion step turns out not to be rate-determining.

Though papers of experimental studies on these complexes exist in the literature, we have not encountered a systematic computational study. The aim of this study is to understand the effect of different R groups and find a trend for different metal and/or halogen complexes if any.

A systematic approach altering the metal M, the halogen X and the substituent R on the phosphorus atom was taken. The transition metals Ni, Pd and Pt which lie on the same group on the periodic table were used as variants for M. The halogens used for X are Cl, Br and I. The choices for R were methyl as a small alkyl group, cyclohexyl as a bulky alkyl group and phenyl as an aromatic group.

The metal atom also varied as Rh which lies on the same period with Pd on the periodic table. Rh complexes of methyl substituted ligand with halogen atoms being Cl and Br were studied.

The N functionality on the backbone of the aminomethylphosphine complexes makes them more soluble compared to the complexes which have C atom on the backbone instead of N atom. The effect of having N atom or C atom on the backbone of the ligand which may cause changes on the geometrical and electronic structure was also examined. The substituent on the N atom can also be varied which may also cause changes on the structure. One example for each of the complexes with C on the backbone and the complex with phenyl substituent on the N atom was examined.

The transition state structures for the ethylene insertion step of the hydrogenation reaction of ethylene were also examined.

2. METHODOLOGY

.

2.1. Semi Empirical Theory

Semi empirical theory [24] uses Hartree-Fock theory, but the number of equations is reduced by making approximations with introduction of parameters related with the experimental results. The semi empirical theory uses only the valance electrons; the core electrons are ignored. The main approximation in the semi empirical theory that leads to the decrease of the computational cost is the Neglect of Diatomic Differential Overlap (NDDO). NDDO approximation states that atomic orbitals located on different atomic centers do not overlap. Thus, NDDO approximation leads to decrease in number of electron-electron interaction terms in Roothaan-Hall equation to N^2 from N^4 where N is the total number of basis functions.

In this work modified neglect of diatomic overlap, parametric method number 3 (PM3) is used to obtain the initial geometries so that the computational cost was reduced.

2.2. Density Functional Theory

The density functional theory is based on the Kohn-Hohenberg theorems proposed in 1964 [25,26]. The first theorem states that the electron density $\rho(r)$ determines the external potential $v(r)$, i.e. the potential due to the nuclei. The second theorem introduces the variational principle. Hence, the electron density can be computed variationally and the position of nuclei, energy, wave function and other related parameters can be calculated [25,26].

The electron density is defined as:

$$\rho(x) = N \int \ldots \int \left|\Psi(x_1, x_2, \ldots x_n)\right|^2 dx_1 dx_2 \ldots dx_n \tag{2.1}$$

where x represents both spin and spatial coordinates of electrons.

The electronic energy can be expressed as a functional of the electron density:

$$E[\rho] = \int v(r)\rho(r)dr + T[\rho] + V_{ee}[\rho] \tag{2.2}$$

where $T[\rho]$ is the kinetic energy of the interacting electrons and $V_{ee}[\rho]$ is the interelectronic interaction energy. The electronic energy may be rewritten as:

$$E[\rho] = \int v(r)\rho(r)dr + T_s[\rho] + J[\rho] + E_{xc}[\rho] \tag{2.3}$$

with $J[\rho]$ being the coulomb energy, $T_s[\rho]$ being the kinetic energy of the non-interacting electrons and $E_{xc}[\rho]$ is the exchange-correlation energy functional. The exchange-correlation functional is expressed as the sum of an exchange functional $E_x[\rho]$ and a correlation functional $E_c[\rho]$, although it contains also a kinetic energy term arising from the kinetic energy difference between the interacting and non-interacting electron systems.

In Kohn-Sham density functional theory, a reference system of independent non-interacting electrons in a common, one-body potential V_{KS} yielding the same density as the real fully-interacting system is considered. More specifically, a set of independent reference orbitals ψ_i satisfying the following independent particle Schrödinger equation are imagined:

$$\left[-\frac{1}{2}\nabla^2 + V_{KS}\right]\psi_i = \varepsilon_i\psi_i \tag{2.4}$$

with the one-body potential V_{KS} defined as:

$$V_{KS} = v(r) + \frac{\partial J[\rho]}{\partial \rho(r)} + \frac{\partial E_{xc}[\rho]}{\partial \rho(r)} \tag{2.5}$$

$$V_{KS} = v(r) + \frac{\rho(r')}{|r - r'|}dr' + v_{xc}(r) \tag{2.6}$$

where $v_{xc}(r)$ is the exchange-correlation potential. The independent orbitals ψ_i are known as Kohn-Sham orbitals and give the exact density by:

$$\rho(r) = \sum_{i}^{N} |\psi_i|^2 \tag{2.7}$$

if the exact form of the exchange-correlation functional is known. However, the exact form of this functional is not known and approximate forms are developed starting with the local density approximation (LDA). LDA treats the electron density as constant or varying slightly through the molecule and does not take the spins of two electrons in the same Kohn-Sham orbital. The most recently used DFT methods use the Becke three-parameter Lee-Yang-Parr (B3LYP), which is a gradient corrected functional that assigns orbitals by considering the spins of the electrons.

2.3. Basis Set

The Los Alamos National Laboratory Double Zeta (LANL2DZ) basis set which is applicable to metals of interest, treats the chemically inert core electrons with an effective core potential (ECP). The valence shell is split into two in this basis set [27-29].

The conformer searches for the free ligands and the transition metal complexes were done with the semi empirical method PM3 in the program package SPARTAN'04 [30]. The density functional theory (DFT) was used to optimize the structures to higher levels. As the DFT functional, Becke 3-parameter-Lee-Yang-Parr exchange-correlation functional (B3LYP) [31,32] which is found in the program package GAUSSIAN98 [33] was used. B3LYP functional was chosen because it was successfully applied to the metals of interest in the literature.

The optimizations of Ni complexes were first done with the PM3 method. The PM3 optimized structures were then reoptimized by B3LYP functional with LANL2DZ basis set. The rest of the complexes and the transition state structures were optimized by B3LYP functional with LANL2DZ basis set only.

3. RESULT S AND DISCUSSIONS

3.1. The Free Ligands $(R_2PCH_2)_2NMe$

The three free ligands that were optimized are $(Me_2PCH_2)_2NMe$, $(Cy_2PCH_2)_2NMe$ and $(Ph_2PCH_2)_2NMe$ which have methyl, cyclohexyl and phenyl substituents on the phosphorus atoms respectively (Figure 3.1). The optimized structures of $(Me_2PCH_2)_2NMe$, $(Cy_2PCH_2)_2NMe$ and $(Ph_2PCH_2)_2NMe$ were specified by their bond lengths, angles and dihedral angles.

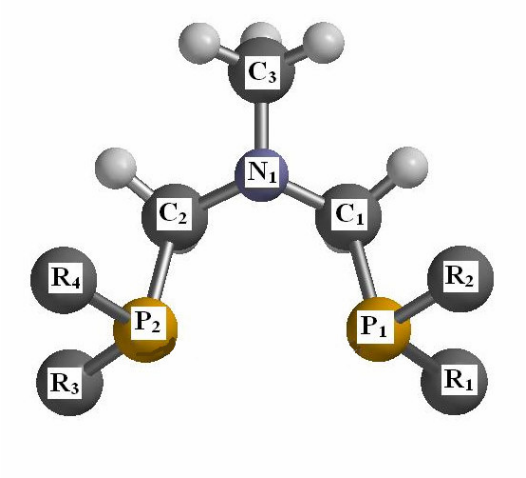

R = Me, Cy, Ph

Figure 3.1. Aminomethylphosphine Ligands

3.1.1. The Structures of $(Me_2PCH_2)_2NMe$, $(Cy_2PCH_2)_2NMe$ and $(Ph_2PCH_2)_2NMe$

The conformer search was done for the free ligand $(Me_2PCH_2)_2NMe$ by the PM3 method. At the end of the conformer search 55 conformers were obtained which were separated by at most 3.78 kcal/mol on the potential energy surface. The conformers having the lone pairs on the phosphorus atoms directed towards each other were chosen because they are more prone to form a complex. Between these structures, the conformer with the lowest energy was taken and reoptimized with the DFT method. The final structure of $(Me_2PCH_2)_2NMe$ is represented in Figure 3.2. The calculated bond lengths, angles, dihedral

angles and the Mulliken charges are shown in Table 3.1, Table 3.2, Table 3.3 and Table 3.4. The numbering system is given in Figure 3.1.

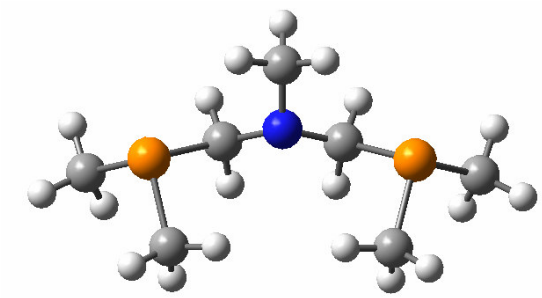

Figure 3.2. The DFT optimized structure of $(Me_2PCH_2)_2NMe$

Table 3.1. The calculated bond lengths for the free ligands

Bond	**R**		
	Me	**Cy**	**Ph**
P1-C1	1.929	1.926	1.940
C1-N1	1.476	1.482	1.472
N1-C3	1.476	1.478	1.473
P2-C2	1.929	1.931	1.942
C2-N1	1.476	1.481	1.469
R1-P1	1.905	1.945	1.894
R2-P1	1.909	1.937	1.895
R3-P2	1.905	1.941	1.902
R4-P2	1.909	1.938	1.896

Table 3.2. The calculated bond angles for the free ligands

Angle	R		
	Me	**Cy**	**Ph**
P1-C1-N1	111.69	112.24	111.98
C1-N1-C2	114.24	112.08	114.91
C1-N1-C3	113.09	112.94	113.92
C2-N1-C3	113.09	112.28	114.33
P2-C2-N1	111.69	111.91	112.66
R1-P1-C1	97.96	103.96	100.24
R2-P1-C1	97.33	100.30	97.58
R3-P2-C2	97.96	97.51	98.01
R4-P2-C2	97.33	99.03	101.81
R1-P1-R2	99.67	101.73	102.43
R3-P1-R4	99.67	104.37	102.28

Table 3.3. The calculated dihedral angles for the free ligands

Dihedral	R		
	Me	**Cy**	**Ph**
P1-C1-N1-C3	72.44	65.51	72.83
P1-C1-N1-C2	-156.30	-166.47	-152.52
P2-C2-N1-C3	-72.43	-68.81	-74.65
P2-C2-N1-C1	156.30	162.82	150.88
R1-P1-C1-N1	78.18	82.99	81.66
R2-P1-C1-N1	179.07	-172.06	-174.18
R3-P2-C2-N1	-78.17	-82.01	-159.91
R4-P2-C2-N1	-179.06	172.06	95.68

Table 3.4. The calculated Mulliken Charges for the free ligands

	R		
	Me	**Cy**	**Ph**
P1	0.619	0.653	0.648
P2	0.619	0.626	0.651
R1	-0.197	-0.202	-0.215
R2	-0.216	-0.220	-0.248
R3	-0.197	-0.193	-0.233
R4	-0.216	-0.202	-0.249
$N(Me)(CH_2)_2$	-0.409	-0.464	-0.356

Similarly, the conformer search for the free ligand $(Cy_2PCH_2)_2NMe$ was done. As the result of the conformer search 74 conformers were obtained which were separated with 1.85-9.98 kcal/mol on the potential energy surface. These conformers include the structures with cyclohexyl groups bonded to phosphorous atoms by their axial positions, cyclohexyl groups bonded to phosphorus atoms by their equatorial positions and the structures with cyclohexyl groups in boat form. The conformer which has the lone pairs on the phosphorus atoms directed towards each other was chosen from the conformers with cyclohexyl groups bonded to the phosphorus atoms by their equatorial positions. Then, it was reoptimized with the DFT method. The optimized structure and the X-ray crystal structure [34] of $(Cy_2PCH_2)_2NMe$ are represented in Figure 3.3. The bond lengths and the angles for the experimental and calculated structures are shown in Table 3.5 and Table 3.6 respectively. The calculated bond lengths, the bond angles, the dihedral angles and the Mulliken charges are shown in Table 3.1, Table 3.2, Table 3.3 and Table 3.4 respectively. The conformation of the optimized structure matches well with the X-ray crystal structure's conformation. The bond lengths calculated by LANL2DZ basis set give longer bond lengths then experiments.

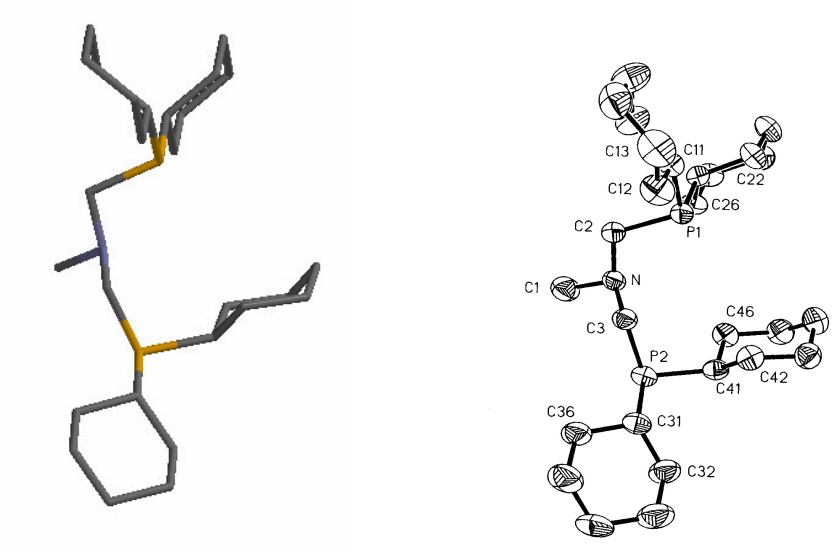

(a) (b)

Figure 3.3. The DFT optimized (a) and the X-ray crystal (b) [34] structures of $(Cy_2PCH_2)_2NMe$

Table 3.5. The experimental [34] and the calculated bond lengths for the free ligand $(Cy_2PCH_2)_2NMe$

Bond	**Exp.**	**Calc.**
P1-C1	1.860 (3)	1.926
C1-N1	1.458 (3)	1.482
N1-C3	1.460 (4)	1.478
P2-C2	1.857 (3)	1.931
C2-N1	1.468 (3)	1.481
R1-P1	1.865 (3)	1.945
R2-P1	1.863 (3)	1.937
R3-P2	1.855 (3)	1.941
R4-P3	1.861 (3)	1.938

Table 3.6. The experimental [34] and the calculated angles for the free ligand $(Cy_2PCH_2)_2NMe$

Angle	Exp.	Calc.
P1-C1-N1		112.2
C1-N1-C2	111.2 (2)	112.1
C1-N1-C3	110.8 (2)	112.9
C2-N1-C3	110.0 (2)	112.3
P2-C2-N1		111.9
R1-P1-C1	102.4 (1)	104.0
R2-P1-C1	100.5 (1)	100.3
R3-P2-C2	102.3 (1)	97.5
R4-P2-C2	102.3 (1)	99.0
R1-P1-R2	102.6 (1)	101.7
R3-P1-R4	102.4 (1)	104.4

The conformer search for the free ligand $(Ph_2PCH_2)_2NMe$ was done with the PM3 method. As the result of the conformer search 100 conformers were obtained which were separated with at most 4.50 kcal/mol on the potential energy surface. The conformer which has the lone pairs on the phosphorus atoms directed towards each other was chosen to be reoptimized with the DFT method. The optimized structure of $(Ph_2PCH_2)_2NMe$ is represented in Figure 3.4. The calculated bond lengths, the bond angles, the dihedral angles and the Mulliken charges are shown on Table 3.1, Table 3.2, Table 3.3 and Table 3.4.

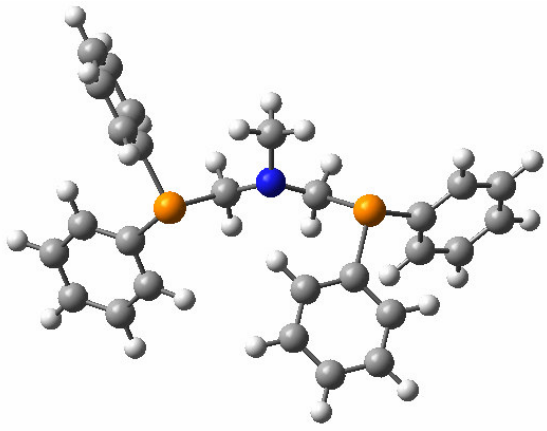

Figure 3.4. The DFT optimized structures of $(Ph_2PCH_2)_2NMe$

3.1.2. The Comparison of the Geometrical Parameters of $(Me_2PCH_2)_2NMe$, $(Cy_2PCH_2)_2NMe$ and $(Ph_2PCH_2)_2NMe$

The phenyl substituted ligand has shorter R-P bond and longer P-C bond than methyl and cyclohexyl substituted ligands. This can be attributed to stronger electron withdrawal by phenyl group. Also interesting to note N1-C1, N1-C2 and N1-C3 distances are all the shortest for the phenyl substituted ligand.

C1-N1-C2, C1-N1-C3 and C2-N1-C3 all have the same trend cy < me < ph. P-C-N angle ranges about 122^0 and is the smallest for the methyl substituted complex. R-P-R angle increases generally as me < ph < cy which is also the trend for the increase of their steric crowding.

One of the R-P-C-N angles for all ligands is close to 180^0 and shows that two of the substituents on each phosphorus atom are directed to the opposite direction to the C-N bond. The other two substituents generally make about 80^0 angles to the C-N bond.

The P atom being less electronegative then C atom is expected to donate electron to C atom on the backbone of the ligand and to the substituents to which it is bonded. The positive charge accumulated on the phosphorus atoms is the largest for phenyl substituted ligand. Parallelly, the negative charge on the phenyl groups is more than those of methyl and cyclohexyl groups. The phosphorus atoms can donate their electrons to the phenyl

groups through a molecular orbital which involves the overlap of p orbital of the phosphorus atom and the π molecular orbital of the phenyl group. There are two of these molecular orbitals HOMO(-9) and HOMO(-10) with very similar in energies, which are shown in Figure 3.5.

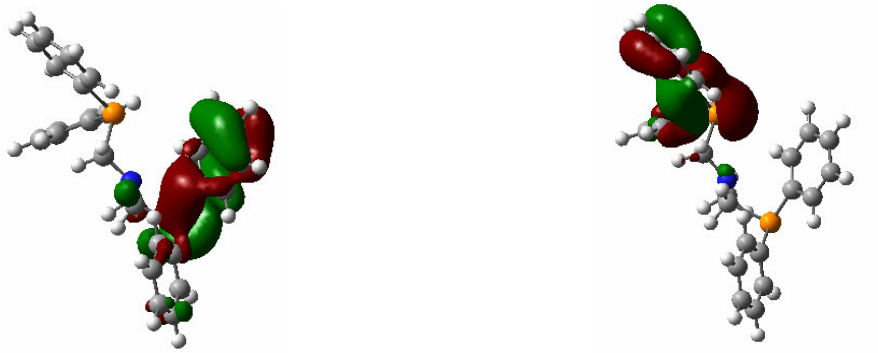

HOMO(-9) HOMO(-10)

Figure 3.5. HOMO(-9) and HOMO(-10) of ligand $(Ph_2PCH_2)_2NMe$

The negative charge on the $(CH_2)_2N(Me)$ fragment, which involves the two methylenes, N atom and the methyl group on the N atom, increases as ph < me < cy.

3.2. The Chlorine Complexes: Ni, Pd and Pt Derivatives of $(Me_2PCH_2)_2NMe$, $(Cy_2PCH_2)_2NMe$ and $(Ph_2PCH_2)_2NMe$

3.2.1. The Structures of the Chlorine Complexes

The conformer search carried out by PM3 method for the complex $[NiCl_2(Me_2PCH_2)_2NMe]$ gave two conformers which have energies -451.68 kcal/mol and -446.31 kcal/mol. The higher energy conformer and the lower energy conformer differ in the direction of the methyl group on the nitrogen atom. The lower energy conformer was taken and reoptimized with DFT method. The final structure of $[NiCl_2(Me_2PCH_2)_2NMe]$ is represented in Figure 3.6. The calculated bond lengths, the bond angles, the dihedral angles and the Mulliken charges are shown in Table 3.7., Table 3.8., Table 3.9. and Table 3.10.

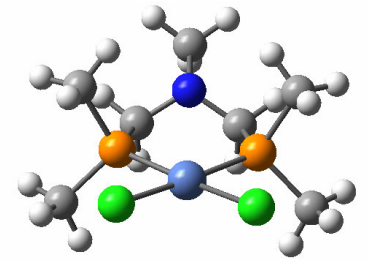

Figure 3.6. The optimized structure of $[NiCl_2(Me_2PCH_2)_2NMe]$

Table 3.7. The calculated bond lengths for $[NiCl_2(Me_2PCH_2)_2NMe]$, $[NiCl_2(Cy_2PCH_2)_2NMe]$ and $[NiCl_2(Ph_2PCH_2)_2NMe]$

Bond	**R**		
	Me	**Cy**	**Ph**
Ni-P1	2.285	2.304	2.300
Ni-P2	2.285	2.304	2.299
Ni-Cl1	2.260	2.269	2.255
Ni-Cl2	2.260	2.269	2.255
P1-C1	1.910	1.914	1.917
C1-N1	1.471	1.472	1.472
N1-C3	1.480	1.481	1.484
P2-C2	1.910	1.914	1.917
C2-N1	1.471	1.472	1.472
R1-P1	1.878	1.914	1.876
R2-P1	1.878	1.926	1.874
R3-P2	1.878	1.914	1.876
R4-P2	1.878	1.926	1.874

Table 3.8. The calculated angles for $[NiCl_2(Me_2PCH_2)_2NMe]$, $[NiCl_2(Cy_2PCH_2)_2NMe]$ and $[NiCl_2(Ph_2PCH_2)_2NMe]$

Angle	**R**		
	Me	**Cy**	**Ph**
Ni-P1-C1	118.74	116.92	118.00
Ni-P2-C2	118.74	117.03	117.99
Ni-P1-R1	115.40	112.03	117.00
Ni-P1-R2	111.32	117.18	112.39
Ni-P2-R3	115.40	112.01	116.99
Ni-P2-R4	111.32	117.19	112.40
Cl1-Ni-P1	84.87	85.64	85.77
Cl2-Ni-P2	84.87	85.66	85.77
Cl1-Ni-Cl2	95.49	92.55	93.59
P1-Ni-P2	94.66	96.10	94.83
P1-C1-N1	112.81	114.09	114.68
C1-N1-C2	113.52	113.37	113.26
C1-N1-C3	113.88	113.05	112.77
C2-N1-C3	113.88	113.03	112.77
P2-C2-N1	112.81	114.15	114.68
R1-P1-C1	101.70	101.94	98.48
R2-P1-C1	102.64	100.94	102.79
R3-P2-C2	101.70	101.95	98.48
R4-P2-C2	102.64	100.89	102.79
R1-P1-R2	105.43	106.05	106.27
R3-P2-R4	105.43	105.99	106.27

Table 3.9. The calculated angles for $[NiCl_2(Me_2PCH_2)_2NMe]$, $[NiCl_2(Cy_2PCH_2)_2NMe]$, and $[NiCl_2(Ph_2PCH_2)_2NMe]$

Dihedral	R		
	Me	**Cy**	**Ph**
Ni-P1-C1-N1	39.02	-39.29	40.83
Ni-P2-C2-N1	-39.02	39.91	-40.86
Cl1-Ni-P1-R1	53.78	-53.03	53.94
Cl1-Ni-P1-R2	-66.32	-69.86	-69.43
Cl2-Ni-P2-R3	-53.78	-52.99	-53.95
Cl2-Ni-P2-R4	66.32	69.80	69.43
Cl1-Ni-P1-C1	174.87	170.14	171.22
Cl2-Ni-P2-C2	-174.87	-170.17	-171.22
P1-C1-N1-C3	147.63	149.73	152.73
P1-C1-N1-C2	-79.87	-79.96	-77.67
P2-C2-N1-C3	-147.63	150.10	-152.72
P2-C2-N1-C1	79.87	79.58	77.69
R1-P1-C1-N1	166.84	162.41	167.64
R2-P1-C1-N1	-84.21	-88.40	-83.44
R3-P2-C2-N1	-166.84	-161.83	-167.66
R4-P2-C2-N1	84.21	89.06	83.42

Table 3.10. The Mulliken charges for $[NiCl_2(Me_2PCH_2)_2NMe]$, $[NiCl_2(Cy_2PCH_2)_2NMe]$ and $[NiCl_2(Ph_2PCH_2)_2NMe]$

	R		
	Me	**Cy**	**Ph**
Ni	-0.229	-0.338	-0.236
Cl1	-0.313	-0.296	-0.277
Cl2	-0.313	-0.296	-0.277
P1	0.743	0.750	0.713
P2	0.743	0.750	0.713
R1	-0.087	-0.033	-0.074
R2	-0.072	-0.045	-0.076
R3	-0.087	-0.033	-0.074
R4	-0.072	-0.044	-0.075
$N(Me)(CH_2)_2$	-0.317	-0.409	-0.334

The PM3 conformer search for the $[NiCl_2(Cy_2PCH_2)_2NMe]$ complex gave 96 conformers which were separated by at most 10 kcal/mol on the potential energy surface. These conformers consist of structures with cyclohexyl groups in boat form and structures with cyclohexyl groups bonded to phosphorus atoms from their axial and equatorial positions. The conformer that has the lowest energy was chosen from the structures with cyclohexyl groups bonded to phosphorus atoms from their equatorial positions. It was reoptimized by making use of the DFT method. The optimized structure and the X-ray crystal structure [34] of $[NiCl_2(Cy_2PCH_2)_2NMe]$ are represented in Figure 3.7. The bond lengths and the bond angles for the experimental and the calculated structures are shown in Table 3.11 and Table 3.12. The calculated dihedral angles and the Mulliken charges are shown in Table 3.9 and Table 3.10. The optimized structure matches well with the X-ray crystal structure in terms of conformation.

Table 3.11. The bond lengths for the X-ray [34] and the calculated structures of $[NiCl_2(Cy_2PCH_2)_2NMe]$

Bond	**Exp.**	**Calc.**
Ni-P1	2.137 (2)	2.304
Ni-P2	2.168 (2)	2.304
Ni-Cl1	2.210 (2)	2.269
Ni-Cl2	2.231 (2)	2.269
P1-C1	1.853 (9)	1.914
C1-N1	1.396 (11)	1.472
N1-C3	1.498 (11)	1.481
P2-C2	1.851 (9)	1.914
C2-N1	1.485 (11)	1.472
R1-P1	1.836 (7)	1.914
R2-P1	1.842 (8)	1.926
R3-P2	1.848 (8)	1.914
R4-P2	1.837 (8)	1.926

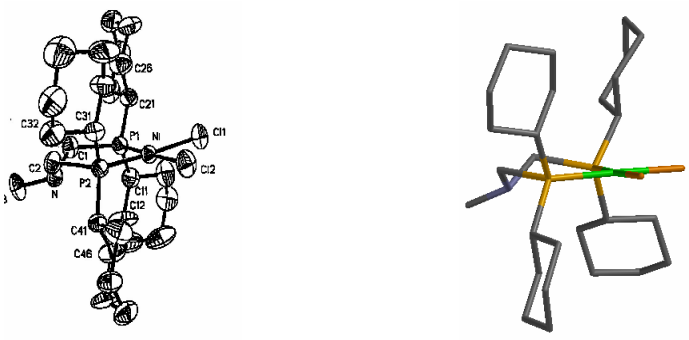

(a) (b)

Figure 3.7. The experimental [34] (a) and the DFT optimized (b) structures for the $[NiCl_2(Cy_2PCH_2)_2NMe]$

Table 3.12. The angles for the X-ray [34] and the calculated structures of $[NiCl_2(Cy_2PCH_2)_2NMe]$

Angle	Exp.	Calc.
Ni-P1-C1	117.2 (3)	116.92
Ni-P2-C2	117.8 (3)	117.03
Ni-P1-R1		112.03
Ni-P1-R2		117.18
Ni-P2-R3		112.01
Ni-P2-R4		117.19
Cl1-Ni-P1	86.8 (1)	85.64
Cl2-Ni-P2	86.2 (1)	85.66
Cl1-Ni-Cl2	89.2(1)	92.55
P1-Ni-P2	97.9 (1)	96.1
P1-C1-N1	113.0 (6)	114.09
C1-N1-C2	111.3 (7)	113.37
C1-N1-C3	110.0 (7)	113.05
C2-N1-C3	107.1 (7)	113.03
P2-C2-N1	112.2 (5)	114.15
R1-P1-C1		101.94
R2-P1-C1		100.94
R3-P2-C2		101.95
R4-P2-C2		100.89

The PM3 conformer search for the $[NiCl_2(Ph_2PCH_2)_2NMe]$ complex gave 53 conformers which were separated by at most 2.2 kcal/mol on the potential energy surface. The conformer with the lowest energy was taken and reoptimized with the DFT method. The optimized structure and the X-ray crystal structure [34] of $[NiCl_2(Ph_2PCH_2)_2NMe]$ are represented in Figure 3.8. The bond lengths and the bond angles for the experimental and the calculated structures are shown in Table 3.13 and Table 3.14. The calculated dihedral angles and the Mulliken charges are shown in Table 3.9 and Table 3.10. The optimized structure matches well with the X-ray crystal structure.

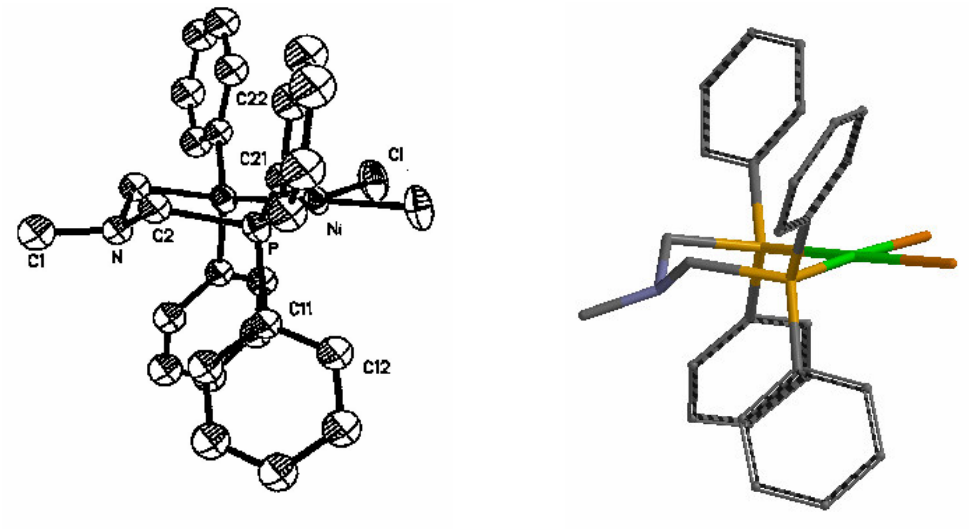

(a) (b)

Figure 3.8. The experimental (a) [34] and the DFT optimized (b) structures for the $[NiCl_2(Ph_2PCH_2)_2NMe]$

Ni-P bond length has the trend cy > ph > me; cy, ph and me referring to the Ni-P distance for $[NiCl_2(Cy_2PCH_2)_2NMe]$, $[NiCl_2(Ph_2PCH_2)_2NMe]$ and $[NiCl_2(Me_2PCH_2)_2NMe]$ complexes respectively. Similar notation is used throughout this thesis for the comparison of other geometrical parameters and charges for all complexes and transition state structures: cy, ph and me referring to the complexes having cyclohexyl, methyl and phenyl substituents on the P atom.

Table 3.13. The bond lengths for the X-ray [34] and the calculated structures of $[NiCl_2(Ph_2PCH_2)_2NMe]$

Bond	Exp.	Calc.
Ni-P1	2.166 (1)	2.300
Ni-P2		2.299
Ni-Cl1		2.255
Ni-Cl2		2.255
P1-C1	1.863 (5)	1.917
C1-N1	1.454 (5)	1.472
N1-C3	1.488 (10)	1.484
P2-C2		1.917
C2-N1		1.472
R1-P1	1.837 (3)	1.876
R2-P1	1.851 (3)	1.874
R3-P2		1.876
R4-P2		1.874

The Ni-Cl bond length has the trend cy > me > ph for different R groups which is also the trend for the R-P bond length. P-C bond length has the trend ph > cy > me. R-P and P-C bond lengths of the Ni complexes have the same trends with the free ligands. The Ni atom forms a square planar geometry with chlorine atoms and phosphorus ends of the ligand. The Cl-Ni-Cl angle and Cl-Ni-P angle are close to 90° which is typical for a square planar geometry. The bite angle P-M-P is the largest for the cyclohexyl substituted complex with 96.10° and the smallest for the methyl substituted complex with 94.66°. R-P-R angle has the trend me < cy < ph. Upon complexation, R-P-R angle enlarges for all Ni complexes of which the methyl substituted complex has the most enlargements. Ni-P-C-N dihedral angle is close to 40 for all of them and is symmetric for the methyl and phenyl substituted complexes. Ni-P-C-N dihedral angle has the trend as ph > cy > me.

Table 3.14. The angles for the X-ray [34] and the calculated structures of $[NiCl_2(Ph_2PCH_2)_2NMe]$

Angle	Exp.	Calc.
Ni-P1-C1		118
Ni-P2-C2	119.5 (2)	117.99
Ni-P1-R1		117
Ni-P1-R2		112.39
Ni-P2-R3		116.99
Ni-P2-R4		112.4
Cl1-Ni-P1		85.77
Cl2-Ni-P2		85.77
Cl1-Ni-Cl2	91.9 (1)	93.59
P1-Ni-P2	92.9 (1)	94.83
P1-C1-N1	114.4 (4)	114.68
C1-N1-C2	111.0 (5)	113.26
C1-N1-C3		112.77
C2-N1-C3		112.77
P2-C2-N1		114.68
R1-P1-C1		98.48
R2-P1-C1		102.79
R3-P2-C2		98.48
R4-P2-C2		102.79

In comparison to the free ligands the positive charge on P atoms increases and the negative charge on the R groups decreases significantly. The charge on the R groups is similar for methyl and phenyl groups and the least for cyclohexyl groups having the trend cy < ph < me. The negative charge on Ni atom has the trend cy > ph ≈ me. The positive charge on P atoms has the trend cy ≈ me > ph. Compared to the free ligand the total negative charge on the $N(me)(CH_2)_2$ fragment decreases. This decrease is the largest for methyl complex, next for cyclohexyl complex and the least for phenyl complex.

The structures of the Pd and Pt complexes of $(Me_2PCH_2)_2NMe$, $(Cy_2PCH_2)_2NMe$ and $(Ph_2PCH_2)_2NMe$ were obtained by taking the same coordinates of the Ni complexes, replacing the metal center with the Pd or Pt atoms and finally reoptimizing with the DFT

method. The structures of the Pd and Pt complexes of $(Me_2PCH_2)_2NMe$, $(Cy_2PCH_2)_2NMe$ and $(Ph_2PCH_2)_2NMe$ ligands are shown in Figure 3.9 and Figure 3.10. The calculated bond lengths, the bond angles, the dihedral angles and the Mulliken charges are shown in Table 3.15, Table 3.16, Table 3.17 and Table 3.18 for the Pd complexes and in Table 3.19, 3.20, 3.21 and 3.22 for the Pt complexes.

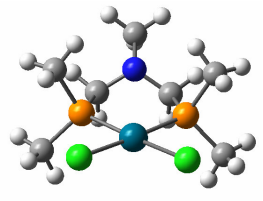

(a)

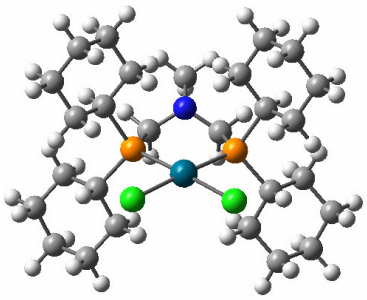

(b)

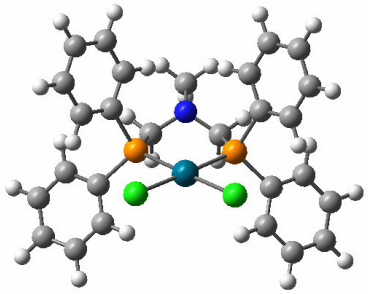

(c)

Figure 3.9. The structures of $[PdCl_2(Me_2PCH_2)_2NMe]$ (a), $[PdCl_2(Cy_2PCH_2)_2NMe]$ (b) and $[PdCl_2(Ph_2PCH_2)_2NMe]$ (c)

Table 3.15. The calculated bond lengths for $[PdCl_2(Me_2PCH_2)_2NMe]$, $[PdCl_2(Cy_2PCH_2)_2NMe]$ and $[PdCl_2(Ph_2PCH_2)_2NMe]$

Bond	R		
	Me	Cy	Ph
Pd-P1	2.363	2.383	2.379
Pd-P2	2.363	2.383	2.379
Pd-Cl1	2.426	2.432	2.419
Pd-Cl2	2.426	2.432	2.419
P1-C1	1.909	1.912	1.915
C1-N1	1.471	1.473	1.472
N1-C3	1.48	1.481	1.484
P2-C2	1.909	1.912	1.915
C2-N1	1.471	1.472	1.472
R1-P1	1.877	1.914	1.875
R2-P1	1.876	1.922	1.871
R3-P2	1.877	1.914	1.875
R4-P2	1.876	1.922	1.871

For the Pd complexes Pd-P bond length shows the same trend cy > ph > me as that of Ni complexes. The Pd-Cl and R-P bond lengths have the trend cy > me > ph which is also the same trend for Ni complexes. Similar to the Ni complexes, P-C has the trend ph > cy > me also for the Pd complexes. The trends for R-P and P-C bond lengths are the same with the free ligands also.

Cl-Pd-Cl angles are larger and compared to the Ni complexes. Cl-Pd-P angles are smaller compared to the Ni complexes. These Cl-Pd-P and Cl-Pd-Cl angles, which are close to 90°, again show a square planar formation around the Pd atoms. The bite angle P-Pd-P is the largest for the cyclohexyl substituted complex with 95.72° and the smallest for the phenyl substituted complex with 94.93°. R-P-R angles of Pd complexes have the same trend with those of Ni complexes as me < cy < ph and enlarge most for the methyl complex compared to the free ligands.

Table 3.16. The calculated angles for $[PdCl_2(Me_2PCH_2)_2NMe]$, $[PdCl_2(Cy_2PCH_2)_2NMe]$ and $[PdCl_2(Ph_2PCH_2)_2NMe]$

Angle	**R**		
	Me	**Cy**	**Ph**
Pd-P1-C1	116.53	115.36	116.07
Pd-P2-C2	116.53	115.4	116.07
Pd-P1-R1	115.34	111.87	117.02
Pd-P1-R2	111.71	117.15	112.93
Pd-P2-R3	115.34	111.86	117.02
Pd-P2-R4	111.71	117.15	112.93
Cl1-Pd-P1	83.96	85.75	85.71
Cl2-Pd-P2	83.96	85.75	85.71
Cl1-Pd-Cl2	96.73	92.72	93.61
P1-Pd-P2	95.26	95.72	94.93
P1-C1-N1	113.09	114.58	115.11
C1-N1-C2	114.15	114.08	113.8
C1-N1-C3	114.29	113.21	112.9
C2-N1-C3	114.29	113.2	112.9
P2-C2-N1	113.09	114.6	115.11
R1-P1-C1	102.77	102.56	99.15
R2-P1-C1	103.75	102.22	103.72
R3-P2-C2	102.77	102.56	99.15
R4-P2-C2	103.75	102.19	103.72
R1-P1-R2	105.44	106.05	106.27
R3-P2-R4	105.43	105.99	106.27

Pd-P-C-N dihedral angle ranges about 40° and is symmetric for the methyl and phenyl substituted complexes. Pd-P-C-N dihedral angles have the trend as ph > cy > me.

The negative charge on Pd was found to be larger than the negative charge on Ni and has the trend cy > ph > me.

The positive charge on P for Pd complex was found to be larger than those for Ni complexes and having the trend cy > me > ph. The charge on the R groups, having the same trend cy < ph < me with Ni complexes, is again similar for methyl and phenyl groups and the least for cyclohexyl groups. The total charge on the $N(Me)(CH_2)_2$ fragment is lower than that of Ni complexes and has the trend as cy > ph > me. Decrease of the negative charge on the backbone of the ligand is the largest for methyl substituted complexes. Upon complexation the positive charge on the P atoms increases whereas the negative charge on the R groups and the $N(Me)(CH_2)_2$ fragment decreases.

Table 3.17. The calculated dihedral angles for $[PdCl_2(Me_2PCH_2)_2NMe]$, $[PdCl_2(Cy_2PCH_2)_2NMe]$ and $[PdCl_2(Ph_2PCH_2)_2NMe]$

Dihedral	**R**		
	Me	**Cy**	**Ph**
Pd-P1-C1-N1	39.28	41.63	41.89
Pd-P2-C2-N1	-39.28	-41.43	-41.89
Cl1-Pd-P1-R1	54.13	50.56	53.69
Cl1-Pd-P1-R2	-66.25	-72.32	-70.09
Cl2-Pd-P2-R3	-54.13	-50.57	-53.70
Cl2-Pd-P2-R4	66.25	72.29	70.08
Cl1-Pd-P1-C1	174.77	167.27	170.33
Cl2-Pd-P2-C2	-174.77	-167.30	-170.33
P1-C1-N1-C3	142.86	146.83	149.38
P1-C1-N1-C2	-82.95	-81.79	-80.24
P2-C2-N1-C3	-142.86	-146.95	-149.38
P2-C2-N1-C1	82.95	81.66	80.24
R1-P1-C1-N1	166.41	163.50	168.13
R2-P1-C1-N1	-83.93	-86.63	-82.58
R3-P2-C2-N1	-166.41	-163.31	-168.12
R4-P2-C2-N1	83.93	86.84	82.59

Table 3.18. The Mulliken charges for $[PdCl_2(Me_2PCH_2)_2NMe]$, $[PdCl_2(Cy_2PCH_2)_2NMe]$ and $[PdCl_2(Ph_2PCH_2)_2NMe]$

	R		
	Me	**Cy**	**Ph**
Pd	-0.304	-0.442	-0.313
Cl1	-0.322	-0.305	-0.286
Cl2	-0.322	-0.305	-0.286
P1	0.762	0.792	0.739
P2	0.762	0.792	0.739
R1	-0.077	-0.029	-0.073
R2	-0.066	-0.043	-0.067
R3	-0.077	-0.028	-0.073
R4	-0.066	-0.043	-0.067
$N(Me)(CH_2)_2$	-0.286	-0.388	-0.310

The trends observed for the Pt complexes are very similar to those for the Ni and Pd complexes. Pt-P bond length with the trend cy > ph > me, Pt-Cl and R-P bond lengths with the same trend cy > me > ph and P-C bond length having the trend ph > cy > me are the same trends with Ni and Pd complexes; R-P and P-C trends being the same with the free ligands also.

The Cl-Pt-Cl and the Cl-Pt-P angles, having values close to 90°, once again indicate a square planar geometry around the metal center. The bite angle P-Pt-P is the largest for the cyclohexyl substituted complex with 96.77° and the smallest for the phenyl substituted complex with 95.43°. The bite angles for the Pt complexes are all larger than those for Ni and Pd analogues. R-P-R angle increases as me < cy < ph which is the same trend with Ni and Pd complexes. Upon complexation R-P-R angle enlarges for all Pt complexes, with methyl substituted complex having the most enlargement.

Pt-P-C-N dihedral angle is again symmetric for the methyl and phenyl substituted complexes and has the same trend ph > cy > me with Ni and Pd complexes.

The negative charge on Pt atom has the trend cy > me > ph. Also it is more negative than the charge on the Pd and Ni . The charge on P atom was found to be less positive than that of the Pd complex and has the trend cy > me > ph. Upon complexation the positive charge on the P atom decreases as ph < cy < me; methyl substituted complex decreasing the most. The charge on the R groups is similar for methyl and phenyl groups and the least for cyclohexyl groups having the same trend cy < ph < me with Ni and Pd complexes. The negative charge on the $N(Me)(CH_2)_2$ fragment has the same trend cy > ph > me with Ni and Pd complexes and smaller than their Ni and Pd analogues. Also, the negative charge on the $N(Me)(CH_2)_2$ fragment decreases upon complexation as ph < cy < me; decreasing the most for the methyl substituted complex.

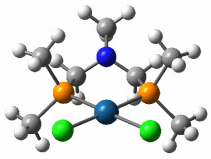

(a)

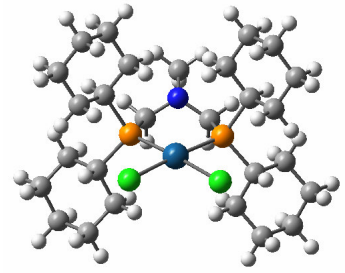

(b)

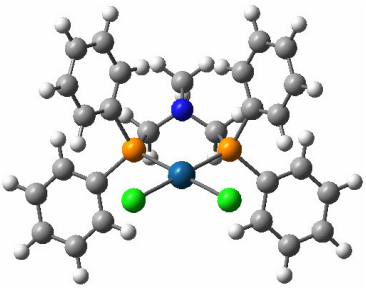

(c)

Figure 3.10. The structures of $[PtCl_2(Me_2PCH_2)_2NMe]$ (a), $[PtCl_2(Cy_2PCH_2)_2NMe]$ (b) and $[PtCl_2(Ph_2PCH_2)_2NMe]$ (c)

Table 3.19. The calculated bond lengths for $[PtCl_2(Me_2PCH_2)_2NMe]$, $[PtCl_2(Cy_2PCH_2)_2NMe]$ and $[PtCl_2(Ph_2PCH_2)_2NMe]$

Bond	R		
	Me	**Cy**	**Ph**
Pt-P1	2.343	2.358	2.352
Pt-P2	2.343	2.358	2.352
Pt-Cl1	2.450	2.457	2.443
Pt-Cl2	2.450	2.457	2.443
P1-C1	1.907	1.909	1.910
C1-N1	1.470	1.472	1.472
N1-C3	1.480	1.480	1.484
P2-C2	1.906	1.909	1.910
C2-N1	1.470	1.472	1.472
R1-P1	1.875	1.913	1.873
R2-P1	1.874	1.920	1.870
R3-P2	1.875	1.913	1.873
R4-P2	1.874	1.920	1.870

Table 3.20. The Mulliken charges for $[PtCl_2(Me_2PCH_2)_2NMe]$, $[PtCl_2(Cy_2PCH_2)_2NMe]$ and $[PtCl_2(Ph_2PCH_2)_2NMe]$

	R		
	Me	**Cy**	**Ph**
Pt	-0.456	-0.557	-0.440
Cl1	-0.274	-0.255	-0.237
Cl2	-0.274	-0.256	-0.237
P1	0.744	0.746	0.694
P2	0.744	0.746	0.694
R1	-0.061	-0.009	-0.030
R2	-0.054	-0.024	-0.063
R3	-0.061	-0.007	-0.030
R4	-0.054	-0.024	-0.063
$N(Me)(CH_2)_2$	-0.252	-0.365	-0.283

Table 3.21. The calculated angles for $[PtCl_2(Me_2PCH_2)_2NMe]$, $[PtCl_2(Cy_2PCH_2)_2NMe]$ and $[PtCl_2(Ph_2PCH_2)_2NMe]$

Angle	R		
	Me	**Cy**	**Ph**
Pt-P1-C1	115.57	114.84	115.49
Pt-P2-C2	115.57	114.87	115.49
Pt-P1-R1	115.22	112.01	116.37
Pt-P1-R2	111.99	116.98	113.15
Pt-P2-R3	115.22	112.00	116.38
Pt-P2-R4	111.99	116.98	113.15
Cl1-Pt-P1	84.72	86.43	86.74
Cl2-Pt-P2	84.72	86.43	86.75
Cl1-Pt-Cl2	93.93	90.32	91.00
P1-Pt-P2	96.55	96.77	95.43
P1-C1-N1	113.15	114.58	115.47
C1-N1-C2	114.09	113.96	113.81
C1-N1-C3	114.43	113.29	112.68
C2-N1-C3	114.43	113.29	112.68
P2-C2-N1	113.15	114.60	115.48
R1-P1-C1	102.95	102.77	99.11
R2-P1-C1	104.26	102.66	104.68
R3-P2-C2	102.95	102.77	99.11
R4-P2-C2	104.26	102.64	104.67
R1-P1-R2	105.67	106.14	106.48
R3-P2-R4	105.67	106.13	106.47

Table 3.22. The calculated dihedral angles for $[PtCl_2(Me_2PCH_2)_2NMe]$, $[PtCl_2(Cy_2PCH_2)_2NMe]$ and $[PtCl_2(Ph_2PCH_2)_2NMe]$

Dihedral	R		
	Me	Cy	Ph
Pt-P1-C1-N1	40.58	41.93	44.83
Pt-P2-C2-N1	-40.58	-41.77	-44.83
Cl1-Pt-P1-R1	52.78	50.20	50.60
Cl1-Pt-P1-R2	-68.04	-72.63	-73.20
Cl2-Pt-P2-R3	-52.78	-50.22	-50.60
Cl2-Pt-P2-R4	68.04	72.60	73.20
Cl1-Pt-P1-C1	172.77	166.93	166.20
Cl2-Pt-P2-C2	-172.77	-166.96	-166.20
P1-C1-N1-C3	142.36	146.83	151.21
P1-C1-N1-C2	-83.15	-81.70	-78.92
P2-C2-N1-C3	-142.36	-146.93	-151.21
P2-C2-N1-C1	83.15	81.60	78.92
R1-P1-C1-N1	167.07	163.81	169.91
R2-P1-C1-N1	-82.78	-86.12	-80.27
R3-P2-C2-N1	-167.07	-163.67	169.92
R4-P2-C2-N1	82.78	86.29	80.28

3.2.2. The Comparison of the Chlorine Complexes of the Ni, Pd and Pt derivatives of $(Me_2PCH_2)_2NMe$, $(Cy_2PCH_2)_2NMe$ and $(Ph_2PCH_2)_2NMe$

Nickel, Palladium and Platinum complexes all have the same following trends for different R substituents:

- M-Cl bond → cy > me > ph
- M-P bond → cy > ph > me
- P-C bond → ph > cy > me
- R-P bond → cy > me > ph

R-P and P-C trends for the complexes are the same with the free ligands also.

The methyl, cyclohexyl and the phenyl complexes all have the same following trends for different metals:

- M-Cl bond → Pt > Pd > Ni
- M-P bond → Pd > Pt > Ni
- P-C bond → Ni ≥ Pd ≥ Pt
- R-P bond → Ni ≥ Pd ≥ Pt

M-P bonds are the longest for Pd with the order Pd > Pt > Ni. With this unexpected trend calculations for $(CO)_2PdCl_2$ and $(CO)_2PtCl_2$ complexes were done to check if the same trend would be observed. Pd-CO bond distances (1.957 Å) are longer than Pt-CO (1.911 Å). A similar case for Pt being smaller than Pd is reported for their methyl-based covalent radii [35]. Also Au is reported to be smaller than Ag in numerous cases [36-40] and specificly for M-phosphine bonds [41].

From Ni to Pd to Pt which is also their order down the group on the periodic table, the atomic radius increases and the M-Cl distance increases. P-C and R-P distances are very close to each other for all complexes.

The bite angles are tabulated in Table 3.23 separately.

Table 3.23. The calculated bite angles for the Cl complexes

	R		
	Cy	**Ph**	**Me**
Ni	96.10	94.83	94.66
Pd	95.72	94.93	95.26
Pt	96.77	95.43	96.55

The bite angle generally increases as Ni < Pd < Pt which is also the trend for the radius of the metals. The cyclohexyl substituted complexes have larger bite angles

compared to their methyl and phenyl substituted analogues. $[PtCl_2(Cy_2PCH_2)_2NMe]$ complex has the largest bite angle with 96.77° and $[NiCl_2(Me_2PCH_2)_2NMe]$ complex has the smallest bite angle with 94.66°. Cl-M-Cl angle increases as cy < ph < me for each complex series of Ni, Pd and Pt and as Pt < Ni < Pd for each complex series of methyl, cyclohexyl and phenyl substituents. R-P-R angle increases as me < cy < ph for each complex series of Ni, Pd and Pt and as Ni < Pd < Pt for each complex series of methyl, cyclohexyl and phenyl substituents.

M-P-C-N dihedral angle has the same trend as ph > cy > me for Ni, Pd and Pt complexes and the same trend as Pt > Pd > Ni for methyl, cyclohexyl and phenyl complexes.

For the charges, Nickel, Palladium and Platinum complexes all have the same following trends for different substituents:

- The negative charge on the M → cy > ph > me for Ni and Pd, cy > ph > me for Pt
- The positive charge on the P → cy > me > ph
- The negative charge on the R groups → me > ph > cy
- The negative charge on the $N(Me)(CH_2)_2$ fragment → cy > ph > me

The methyl, cyclohexyl and the phenyl complexes all have the same following trends for different metals:

- The negative charge on the M atom → Pt > Pd > Ni
- The positive charge on the P atom → Pd > Pt > Ni
- The negative charge on the R groups → Ni > Pd > Pt
- The negative charge on the $N(Me)(CH_2)_2$ fragment → Ni > Pd > Pt

Upon complexation, the positive charge on the P atom increases with the trend cy > me > ph; cyclohexyl substituted complex having the most increase. Also the negative charge on the R groups decreases as cy > me > ph and the $N(Me)(CH_2)_2$ fragment decreases with the trend me > ph > cy.

3.3. The Bromine Complexes: Ni, Pd and Pt Derivatives of $(Me_2PCH_2)_2NMe$, $(Cy_2PCH_2)_2NMe$ and $(Ph_2PCH_2)_2NMe$

3.3.1. The Structures of the Bromine Complexes

The structures of the bromine complexes were obtained by taking the coordinates of optimized structures of chlorine complexes, replacing the chlorine atoms with the bromine atoms and reoptimizing them with DFT method. The optimized structures of $[NiBr_2(Me_2PCH_2)_2NMe]$, $[NiBr_2(Cy_2PCH_2)_2NMe]$, $[NiBr_2(Br_2PCH_2)_2NMe]$ are shown in Figure 3.11. The calculated bond lengths, bond angles, dihedral angles and the Mulliken charges are shown in Table 2.24, Table 2.25, Table 2.26 and Table 3.27.

Table 3.24. The calculated bond lengths for $[NiBr_2(Me_2PCH_2)_2NMe]$, $[NiBr_2(Cy_2PCH_2)_2NMe]$ and $[NiBr_2(Ph_2PCH_2)_2NMe]$

Bond	R		
	Me	Cy	Ph
Ni-P1	2.300	2.321	2.315
Ni-P2	2.300	2.321	2.315
Ni-Br1	2.415	2.427	2.409
Ni-Br2	2.415	2.427	2.409
P1-C1	1.912	1.916	1.920
C1-N1	1.470	1.471	1.470
N1-C3	1.480	1.481	1.483
P2-C2	1.912	1.916	1.920
C2-N1	1.470	1.471	1.470
R1-P1	1.881	1.917	1.878
R2-P1	1.879	1.930	1.875
R3-P2	1.881	1.917	1.878
R4-P2	1.879	1.930	1.875

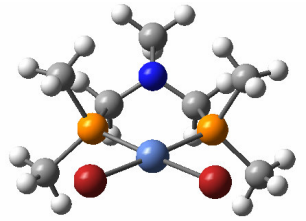

(a)

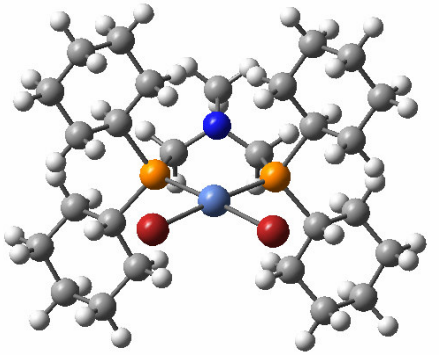

(b)

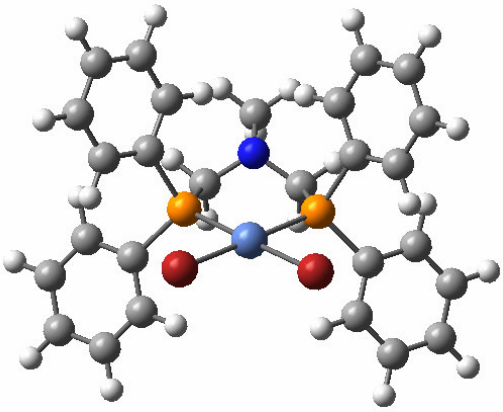

(c)

Figure 3.11. The structures of [$NiBr_2(Me_2PCH_2)_2NMe$] (a), [$NiBr_2(Cy_2PCH_2)_2NMe$] (b) and [$NiBr_2(Ph_2PCH_2)_2NMe$] (c)

Table 3.25. The calculated angles for [$NiBr_2(Me_2PCH_2)_2NMe$], [$NiBr_2(Cy_2PCH_2)_2NMe$] and [$NiBr_2(Ph_2PCH_2)_2NMe$]

Angle	R		
	Me	**Cy**	**Ph**
Ni-P1-C1	118.74	116.72	117.96
Ni-P2-C2	118.74	116.74	117.96
Ni-P1-R1	116.39	112.85	117.22
Ni-P1-R2	111.98	117.71	113.21
Ni-P2-R3	116.39	112.85	117.22
Ni-P2-R4	111.98	117.79	113.21
Br1-Ni-P1	86.18	86.78	86.82
Br2-Ni-P2	86.18	86.81	86.82
Br1-Ni-Br2	93.35	90.55	91.84
P1-Ni-P2	94.17	95.81	94.50
P1-C1-N1	113.05	114.21	114.78
C1-N1-C2	113.33	113.95	113.02
C1-N1-C3	113.94	113.18	112.95
C2-N1-C3	113.94	113.17	112.95
P2-C2-N1	113.05	114.22	114.78
R1-P1-C1	100.62	101.19	97.71
R2-P1-C1	101.87	100.31	102.22
R3-P2-C2	100.62	101.22	97.71
R4-P2-C2	101.87	100.23	102.22
R1-P1-R2	105.34	106.00	106.37
R3-P2-R4	105.34	105.95	106.37

Table 3.26. The dihedral angles for $[NiBr_2(Me_2PCH_2)_2NMe]$, $[NiBr_2(Cy_2PCH_2)_2NMe]$ and $[NiBr_2(Ph_2PCH_2)_2NMe]$

Dihedral	R		
	Me	**Cy**	**Ph**
Ni-P1-C1-N1	39.67	40.01	40.61
Ni-P2-C2-N1	-39.67	-39.86	-40.61
Br1-Ni-P1-R1	53.76	53.74	55.44
Br1-Ni-P1-R2	-67.49	-70.27	-68.98
Br2-Ni-P2-R3	53.76	-53.62	-55.44
Br2-Ni-P2-R4	67.49	70.37	68.98
Br1-Ni-P1-C1	174.20	170.35	171.79
Br2-Ni-P2-C2	-174.20	-170.27	-171.79
P1-C1-N1-C3	147.63	149.17	152.04
P1-C1-N1-C2	-79.92	-80.57	-78.17
P2-C2-N1-C3	-147.63	-149.26	-152.04
P2-C2-N1-C1	79.92	80.49	78.17
R1-P1-C1-N1	167.88	162.88	167.08
R2-P1-C1-N1	-83.79	-88.36	-84.24
R3-P2-C2-N1	-167.88	-162.76	-167.08
R4-P2-C2-N1	83.79	88.55	84.24

Ni-P bond length shows the trend cy > ph > me. Ni-Br bond length and R-P bond length have the same trend cy > me > ph. P-C bond length has the trend ph > cy > me. These trends for the bond lengths of Ni complexes with halogen atoms being Br are the same with the Cl analogues.

Br-Ni-Br angle has the trend me > ph > cy. Br-Ni-Br and Br-Ni-P angles, being close to 90, again show a square planar geometry. The bite angle P-M-P is the largest for the cyclohexyl substituted complex with 95.81° and the smallest for the methyl substituted complex with 94.17°, showing the trend cy > ph > me. R-P-R angles for the Br derivatives of the Ni complexes are about the same with their Cl analogues having the same trend ph > cy > me.

Similar to the Cl derivatives, Ni-P-C-N dihedral angles are also close to 40° and symmetric for the methyl and phenyl substituted complexes. Ni-P-C-N dihedral angle has the same trend as ph > cy > me with the Cl analogues.

The negative charge on Ni has the trend cy > ph > me which is the same trend as the Cl analogues. The positive charge on P atom has the trend cy > ph > me. The negative charge on the R groups has also the same trend me > ph > cy with Cl analogues. The total negative charge on the $N(Me)(CH_2)_2$ fragment has the trend as cy > ph > me. Compared to the Cl complex, the negative charge on Ni now increases, the positive charge on P now decreases and the negative charge on the ligand and the backbone decreases as well.

Table 3.27. The Mulliken charges for $[NiBr_2(Me_2PCH_2)_2NMe]$, $[NiBr_2(Cy_2PCH_2)_2NMe]$ and $[NiBr_2(Ph_2PCH_2)_2NMe]$

	R		
	Methyl	**Cyclohexyl**	**Phenyl**
Ni	-0.278	-0.386	-0.288
Br1	-0.285	-0.274	-0.248
Br2	-0.285	-0.274	-0.248
P1	0.735	0.742	0.705
P2	0.735	0.742	0.705
R1	-0.086	-0.033	-0.075
R2	-0.070	-0.039	-0.074
R3	-0.086	-0.033	-0.075
R4	-0.070	-0.040	-0.074
$N(Me)(CH_2)_2$	-0.311	-0.405	-0.323

The optimized structures of the Palladium complexes $PdBr_2(Me_2PCH_2)_2NMe]$, $[PdBr_2(Cy_2PCH_2)_2NMe]$, $[PdBr_2(Ph_2PCH_2)_2NMe]$ complexes are shown in Figure 3.12. The calculated bond lengths, the bond angles, the dihedral angles and the Mulliken charges are shown in Table 3.28, Table 3.29, Table 3.30 and Table 3.31.

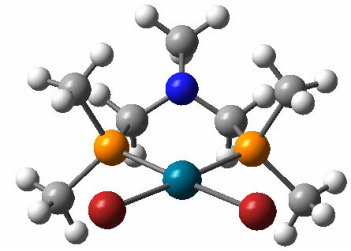

(a)

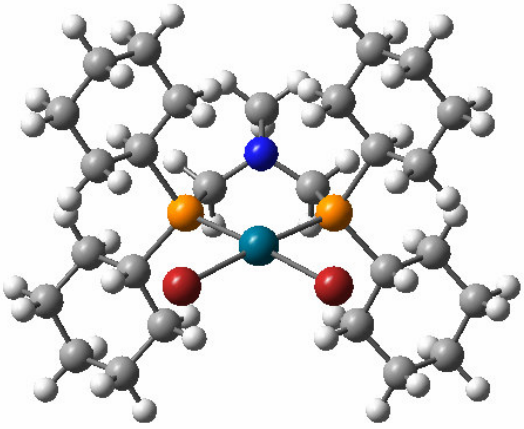

(b)

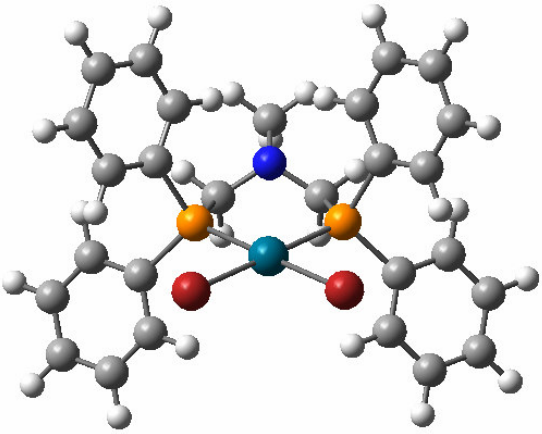

(c)

Figure 3.12. The structures of $[PdBr_2(Me_2PCH_2)_2NMe]$ (a), $[PBrI_2(Cy_2PCH_2)_2NMe]$ (b) and $[PBrI_2(Ph_2PCH_2)_2NMe]$ (c)

Table3.28. The calculated bond lengths for $[PdBr_2(Me_2PCH_2)_2NMe]$, $[PdBr_2(Cy_2PCH_2)_2NMe]$ and $[PdBr_2(Ph_2PCH_2)_2NMe]$

Bond	R		
	Me	Cy	Ph
Pd-P1	2.382	2.403	2.399
Pd-P2	2.382	2.403	2.399
Pd-Br1	2.560	2.569	2.554
Pd-Br2	2.560	2.569	2.554
P1-C1	1.910	1.914	1.918
C1-N1	1.470	1.472	1.471
N1-C3	1.480	1.481	1.484
P2-C2	1.910	1.914	1.918
C2-N1	1.470	1.472	1.471
R1-P1	1.879	1.916	1.876
R2-P1	1.878	1.926	1.872
R3-P2	1.879	1.916	1.876
R4-P2	1.878	1.926	1.872

Pd-P, Pd-Br, R-P and P-C bond lengths for the Br derivatized Pd complexes all have the same trend with their Cl substituted analogues. On the other hand, all the bond lengths, except N1-C3, increase upon changing the halogen from Cl to Br.

The Br-Pd-Br angle was found to be changing between 90.10° and 93.85° and the Br-Pd-P angle also shows the same trend with the Cl and Ni analogues. The bite angle P-M-P is the largest for the cyclohexyl substituted complex with 95.20° and the smallest for the methyl substituted complex with 94.48° having the trend cy > ph ≈ me. R-P-R angle and Pd-P-C-N dihedral angle also show the same trends with their Cl and Ni analogues. On the other hand, Pd-P-C-N dihedral angle enlarges compared to the Ni derivatives.

Table 3.29. The calculated angles for $[PdBr_2(Me_2PCH_2)_2NMe]$, $[PdBr_2(Cy_2PCH_2)_2NMe]$ and $[PdBr_2(Ph_2PCH_2)_2NMe]$

Angle	R		
	Me	**Cy**	**Ph**
Pd-P1-C1	116.72	115.39	115.95
Pd-P2-C2	116.72	115.40	115.95
Pd-P1-R1	116.14	112.60	117.23
Pd-P1-R2	112.30	117.72	113.60
Pd-P2-R3	116.14	112.60	117.23
Pd-P2-R4	112.30	117.73	113.60
Br1-Pd-P1	85.79	87.31	87.08
Br2-Pd-P2	85.79	87.31	87.08
Br1-Pd-Br2	93.85	90.10	91.21
P1-Pd-P2	94.48	95.20	94.58
P1-C1-N1	113.27	114.68	115.23
C1-N1-C2	113.98	113.85	113.59
C1-N1-C3	114.31	113.27	112.91
C2-N1-C3	114.31	113.27	112.91
P2-C2-N1	113.27	114.68	115.23
R1-P1-C1	101.80	101.95	98.58
R2-P1-C1	103.01	101.38	103.22
R3-P2-C2	101.80	101.95	98.58
R4-P2-C2	103.01	101.32	103.22
R1-P1-R2	105.29	106.04	106.33
R3-P2-R4	105.29	106.04	106.33

Table 3.30. The calculated dihedral angles for $[PdBr_2(Me_2PCH_2)_2NMe]$, $[PdBr_2(Cy_2PCH_2)_2NMe]$ and $[PdBr_2(Ph_2PCH_2)_2NMe]$

Dihedral	R		
	Me	Cy	Ph
Pd-P1-C1-N1	39.89	41.42	41.97
Pd-P2-C2-N1	-39.89	-41.40	-41.96
Br1-Pd-P1-R1	54.09	51.22	54.77
Br1-Pd-P1-R2	-67.15	-72.62	-69.98
Br2-Pd-P2-R3	-54.09	-51.20	-54.78
Br2-Pd-P2-R4	67.15	72.64	69.97
Br1-Pd-P1-C1	174.23	167.70	170.68
Br2-Pd-P2-C2	-174.23	-167.68	-170.69
P1-C1-N1-C3	142.96	146.42	148.99
P1-C1-N1-C2	-82.98	-82.26	-80.78
P2-C2-N1-C3	-142.96	-146.43	-148.99
P2-C2-N1-C1	82.98	82.24	80.78
R1-P1-C1-N1	167.41	163.79	167.99
R2-P1-C1-N1	-83.64	-86.91	-82.90
R3-P2-C2-N1	-167.41	-163.77	-167.98
R4-P2-C2-N1	83.64	86.94	82.91

The negative charge on Pd, the positive charge on P, the negative charge on the R groups and the negative charge on the $N(Me)(CH_2)_2$ fragment all have the same trends with the Cl analogues also. Upon changing the Cl atoms with Br atoms, the negative charge on Pd and the negative charge on R groups decrease whereas, the positive charge on P atoms and negative charge on the halogens decrease. The negative charge on the $N(Me)(CH_2)_2$ fragment remain about the same.

Table 3.31. The Mulliken charges for $[PdBr_2(Me_2PCH_2)_2NMe]$, $[PdBr_2(Cy_2PCH_2)_2NMe]$ and $[PdBr_2(Ph_2PCH_2)_2NMe]$

	R		
	Me	**Cy**	**Ph**
Pd	-0.349	-0.483	-0.363
Br1	-0.284	-0.271	-0.245
Br2	-0.284	-0.271	-0.245
P1	0.747	0.779	0.726
P2	0.747	0.779	0.726
R1	-0.079	-0.032	-0.073
R2	-0.067	-0.041	-0.072
R3	-0.079	-0.033	-0.073
R4	-0.067	-0.041	-0.072
$N(Me)(CH_2)_2$	-0.285	-0.388	-0.308

The optimized structures of the platinum complexes $[PtBr_2(Me_2PCH_2)_2NMe]$, $[PtBr_2(Cy_2PCH_2)_2NMe]$, $[PtBr_2(Ph_2PCH_2)_2NMe]$ are shown in Figure 3.13. The calculated bond lengths, bond angles, dihedral angles and the Mulliken charges are shown in Table 3.32, Table 3.33, Table 3.34 and Table 3.35.

Table 3.32. The Mulliken charges for $[PtBr_2(Me_2PCH_2)_2NMe]$, $[PtBr_2(Cy_2PCH_2)_2NMe]$ and $[PtBr_2(Ph_2PCH_2)_2NMe]$

Charge	R		
	Me	**Cy**	**Ph**
Pt	-0.501	-0.603	-0.490
Br1	-0.236	-0.220	-0.197
Br2	-0.236	-0.220	-0.197
P1	0.728	0.734	0.686
P2	0.728	0.734	0.686
R1	-0.062	-0.008	-0.043
R2	-0.054	-0.016	-0.063
R3	-0.062	-0.008	-0.043
R4	-0.054	-0.017	-0.063
$N(Me)(CH_2)_2$	-0.251	-0.367	-0.277

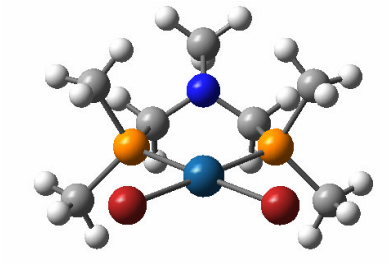

(a)

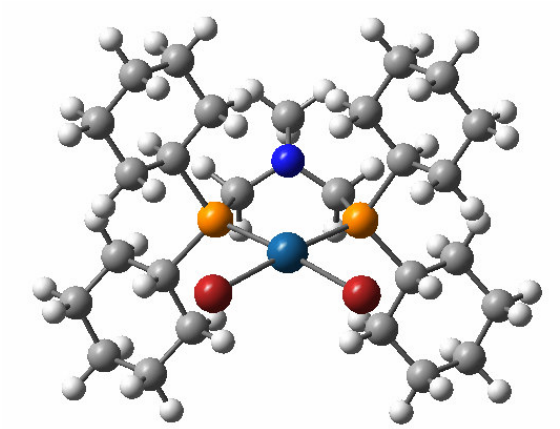

(b)

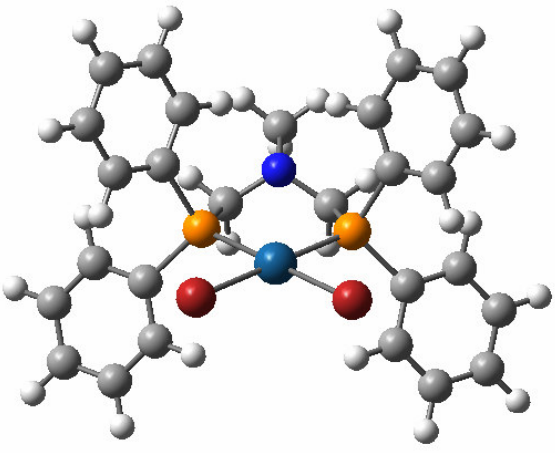

(c)

Figure 3.13. The structures of $[PtBr_2(Me_2PCH_2)_2NMe]$ (a), $[PtBr_2(Cy_2PCH_2)_2NMe]$ (b) and $[PtBr_2(Ph_2PCH_2)_2NMe]$ (c)

For the platinum complexes Pt-P, Pt-Br, R-P, P-C bond lengths, Br-Pt-Br angle, R-P-R angle and Pt-P-C-N dihedral angle have the same trends with their Ni, Pd and Cl analogues. All the bond lengths increase upon changing the halogen atom from Cl to Br. Changing the metal atom from Pd to Pt also results in decreases in all the bond lengths. The bite angle P-M-P is the largest for the cyclohexyl substituted complex with 96.18° and the smallest for the phenyl substituted complex with 95.67°. The bite angles are larger compared to the Ni and Pd analogues. Pt-P-C-N dihedral angles increase compared to the Ni and Pd analogues whereas decrease compared to the Cl analogues.

Table 3.33. The calculated bond lengths for $[PtBr_2(Me_2PCH_2)_2NMe]$, $[PtBr_2(Cy_2PCH_2)_2NMe]$ and $[PtBr_2(Ph_2PCH_2)_2NMe]$

Bond	**R**		
	Me	**Cy**	**Ph**
Pt-P1	2.358	2.374	2.367
Pt-P2	2.358	2.374	2.367
Pt-Br1	2.586	2.593	2.580
Pt-Br2	2.586	2.593	2.580
P1-C1	1.908	1.911	1.914
C1-N1	1.469	1.471	1.471
N1-C3	1.480	1.481	1.484
P2-C2	1.908	1.911	1.914
C2-N1	1.469	1.471	1.471
R1-P1	1.877	1.915	1.873
R2-P1	1.875	1.924	1.872
R3-P2	1.877	1.915	1.873
R4-P2	1.875	1.924	1.872

Table 3.34. The calculated angles for $[PtBr_2(Me_2PCH_2)_2NMe]$, $[PtBr_2(Cy_2PCH_2)_2NMe]$ and $[PtBr_2(Ph_2PCH_2)_2NMe]$

Angle	R		
	Me	**Cy**	**Ph**
Pt-P1-C1	115.96	115.07	115.49
Pt-P2-C2	115.96	115.05	115.50
Pt-P1-R1	115.78	112.63	116.65
Pt-P1-R2	112.42	117.47	113.88
Pt-P2-R3	115.78	117.48	116.65
Pt-P2-R4	112.42	112.63	113.88
Br1-Pt-P1	86.20	87.70	87.29
Br2-Pt-P2	86.20	87.70	87.29
Br1-Pt-Br2	91.78	88.35	89.69
P1-Pt-P2	95.73	96.18	95.67
P1-C1-N1	113.32	114.68	115.18
C1-N1-C2	113.87	113.72	113.34
C1-N1-C3	114.44	113.31	112.98
C2-N1-C3	114.44	113.32	112.98
P2-C2-N1	113.32	114.67	115.18
R1-P1-C1	102.04	102.15	98.83
R2-P1-C1	103.59	101.67	103.55
R3-P2-C2	102.04	102.15	98.83
R4-P2-C2	103.59	101.69	103.56
R1-P1-R2	105.64	106.14	106.60
R3-P2-R4	105.64	106.15	106.60

The negative charge on Pt, the positive charge on P, the negative charge on the R groups and the negative charge on the $N(Me)(CH_2)_2$ fragment all have the same trends with the Ni, Pd and Cl analogues. Upon changing the metal atom from Ni or Pd to Pt, all the charges decrease except the charge on the metal atoms which increases. Upon changing the halogen from Cl to Br, the negative charge on the Pt atom increases, the negative charge on the halogen decrease and the positive charge on the P atoms decreases as well. On the other hand, changing the halogen does not affect the charges on the substituents and on the $N(Me)(CH_2)_2$ fragment; they remain about the same.

Table 3.35. The calculated dihedral angles for $[PtBr_2(Me_2PCH_2)_2NMe]$, $[PtBr_2(Cy_2PCH_2)_2NMe]$ and $[PtBr_2(Ph_2PCH_2)_2NMe]$

Dihedral	**R**		
	Me	**Cy**	**Ph**
Pt-P1-C1-N1	40.51	41.48	42.30
Pt-P2-C2-N1	-40.51	-41.60	-42.29
Br1-Pt-P1-R1	53.67	51.05	55.07
Br1-Pt-P1-R2	-67.88	-72.75	-69.81
Br2-Pt-P2-R3	-53.67	-51.05	-55.07
Br2-Pt-P2-R4	67.88	72.76	69.81
Br1-Pt-P1-C1	173.20	167.59	170.51
Br2-Pt-P2-C2	-173.20	-167.57	-170.52
P1-C1-N1-C3	142.69	146.79	149.17
P1-C1-N1-C2	-83.04	-81.90	-80.67
P2-C2-N1-C3	-142.69	-146.72	-149.18
P2-C2-N1-C1	83.04	81.98	80.66
R1-P1-C1-N1	167.27	163.84	167.54
R2-P1-C1-N1	-83.15	-86.59	82.90
R3-P2-C2-N1	-167.27	-163.95	-167.53
R4-P2-C2-N1	83.15	86.47	82.90

3.3.2. The Comparison of the Bromine Complexes of the Ni, Pt and Pt derivatives of the $(Me_2PCH_2)_2NMe$, $(Cy_2PCH_2)_2NMe$ and $(Ph_2PCH_2)_2NMe$

Ni, Pd and Pt complexes all have the same following trends for different substituents:

- M-P bond → cy > ph > me
- M-Cl bond → cy > me > ph
- P-C bond → ph > cy > me
- R-P bond → cy > me > ph

The methyl, cyclohexyl and the phenyl complexes all have the same following trends for different metals:

- M-P bond → Pd > Pt > Ni
- M-Br bond → Pt > Pd > Ni
- P-C bond → Ni ≥ Pd ≥ Pt
- R-P bond → Ni ≥ Pd ≥ Pt

The bite angles are tabulated in Table 3.36 separately.

Table 3.36. The calculated bite angles for the Br complexes

	R		
	Cy	**Ph**	**Me**
Ni	95.81	94.50	94.17
Pd	95.20	94.58	94.48
Pt	96.18	95.67	95.73

The bite angle generally increases as Ni < Pd < Pt which is also the trend for the radii of the metals. The cyclohexyl substituted complexes have larger bite angles compared to their methyl and phenyl substituted analogues

M-P-C-N dihedral angle has the same trend ph > cy > me for Ni, Pd and Pt complexes and Pt > Pd > Ni for methyl, cyclohexyl and phenyl complexes.

The charges of the Br complexes give the following trends:

- The negative charge on the M atom → cy > ph > me for Pd and Ni
  cy > me > ph for Pt
- The positive charge on the P atom → cy > me > ph.
- The negative charge on the R groups → me > ph > cy
- The negative charge on the $N(Me)(CH_2)_2$ fragment → cy > ph > me

The methyl, cyclohexyl and the phenyl complexes all have the same following trends for different metals:

- The negative charge on the M atom → Pt > Pd > Ni
- The positive charge on the P atom → Pd > Ni > Pt
- The negative charge on the R groups → Ni > Pd > Pt
- The negative charge on the $N(Me)(CH_2)_2$ fragment → Ni > Pd > Pt

Upon complexation, the positive charge on the P atom increases with the trend cy > me > ph; cyclohexyl substituted complex having the most increase.

3.4. The Iodine Complexes: Ni, Pd and Pt Derivatives of $(Me_2PCH_2)_2NMe$, $(Cy_2PCH_2)_2NMe$ and $(Ph_2PCH_2)_2NMe$

3.4.1. The Structures of the Iodine Complexes

The structures of the iodine complexes were obtained by taking the coordinates of optimized structures of chlorine complexes, replacing the chlorine atoms with the iodine atoms and reoptimizing them with DFT method.

The optimized structures of the Nickel complexes of the ligands $(Me_2PCH_2)_2NMe$, $(Cy_2PCH_2)_2NMe$ and $(Ph_2PCH_2)_2NMe$ are shown in Figure 3.14. The calculated bond lengths, bond angles, dihedral angles and the Mulliken charges are shown in Table 3.37, Table 3.38, Table 3.39 and Table 3.40.

Table 3.37. The calculated bond lengths for $[NiI_2(Me_2PCH_2)_2NMe]$, $[NiI_2(Cy_2PCH_2)_2NMe]$ and $[NiI_2(Ph_2PCH_2)_2NMe]$

Bond	**R**		
	Me	**Cy**	**Ph**
Ni-P1	2.316	2.343	2.333
Ni-P2	2.316	2.344	2.333
Ni-I1	2.604	2.619	2.599
Ni-I2	2.604	2.619	2.599
P1-C1	1.913	1.917	1.925
C1-N1	1.468	1.470	1.469
N1-C3	1.480	1.480	1.483
P2-C2	1.913	1.918	1.925
C2-N1	1.468	1.470	1.469
R1-P1	1.884	1.921	1.879
R2-P1	1.881	1.935	1.878
R3-P2	1.884	1.921	1.879
R4-P2	1.881	1.935	1.878

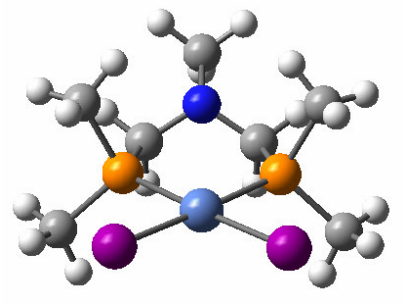

(a)

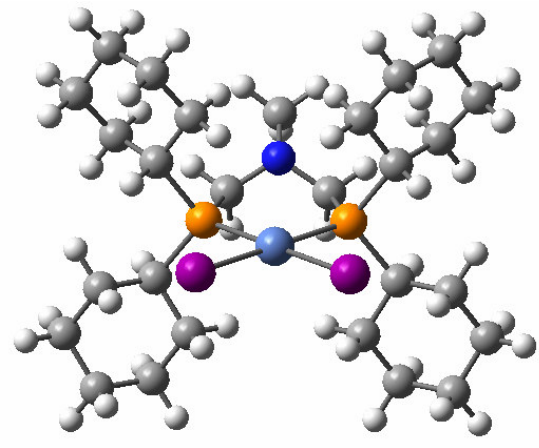

(b)

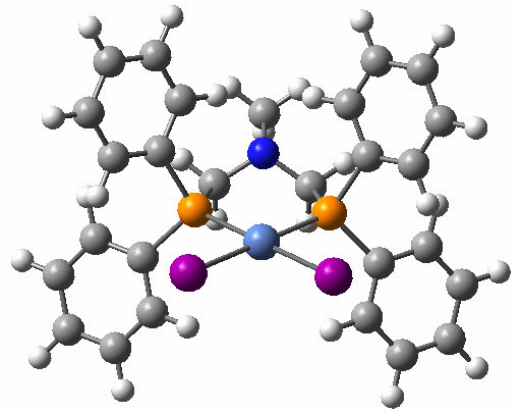

(c)

Figure 3.14. The structures of $[NiI_2(Me_2PCH_2)_2NMe]$ (a), $[NiI_2(Cy_2PCH_2)_2NMe]$ (b) and $[NiI_2(Ph_2PCH_2)_2NMe]$ (c)

Table 3.38. The calculated angles for $[NiI_2(Me_2PCH_2)_2NMe]$, $[NiI_2(Cy_2PCH_2)_2NMe]$ and $[NiI_2(Ph_2PCH_2)_2NMe]$

Angle	R		
	Me	**Cy**	**Ph**
Ni-P1-C1	118.81	116.38	117.97
Ni-P2-C2	118.81	116.66	117.98
Ni-P1-R1	117.75	113.68	117.87
Ni-P1-R2	112.39	118.15	113.68
Ni-P2-R3	117.75	113.74	117.88
Ni-P2-R4	112.39	118.34	113.66
I1-Ni-P1	87.42	87.74	87.81
I2-Ni-P2	87.42	87.98	87.81
I1-Ni-I2	91.51	88.87	90.28
P1-Ni-P2	93.51	95.39	94.05
P1-C1-N1	113.28	114.18	114.86
C1-N1-C2	113.13	112.65	112.84
C1-N1-C3	114.01	113.42	113.10
C2-N1-C3	114.01	113.33	113.10
P2-C2-N1	113.28	114.45	114.87
R1-P1-C1	99.40	100.44	96.97
R2-P1-C1	101.06	99.57	101.37
R3-P2-C2	99.40	100.38	96.96
R4-P2-C2	101.06	99.49	101.37
R1-P1-R2	105.14	106.28	106.53
R3-P2-R4	105.14	105.81	106.53

For the Nickel complexes Ni-P bond length shows the trend cy > ph > me. The Ni-I bond length has the trend cy > me > ph which is also the trend for the R-P bond length. P-C bond length has the trend ph > cy > me. I-Ni-I angle changes between 88.87° and 91.51° and the I-Ni-P angle changes between the 87.42° and 87.98° indicating a square planar

geometry. The bite angle P-M-P is the largest for the cyclohexyl substituted complex with 95.39° and the smallest for the methyl substituted complex with 93.51°. Ni-P-C-N dihedral angles are about 40°.

The negative charge on the Nickel atoms has the trend cy > me > ph. The positive charge on P atoms has the trend cy > me > ph. The negative charge on the $N(Me)(CH_2)_2$ fragment has the trend as cy > ph > me.

Table 3.39. The calculated dihedral angles for $[NiI_2(Me_2PCH_2)_2NMe]$, $[NiI_2(Cy_2PCH_2)_2NMe]$ and $[NiI_2(Ph_2PCH_2)_2NMe]$

Dihedral	**R**		
	Me	**Cy**	**Ph**
Ni-P1-C1-N1	40.62	41.30	40.51
Ni-P2-C2-N1	-40.62	-39.35	-40.48
I1-Ni-P1-R1	53.38	54.71	56.72
I1-Ni-P1-R2	-69.03	-70.88	-68.96
I2-Ni-P2-R3	-53.38	-53.80	-56.68
I2-Ni-P2-R4	69.03	71.32	69.00
I1-Ni-P1-C1	173.37	170.71	172.58
I2-Ni-P2-C2	-173.37	-169.97	-172.55
P1-C1-N1-C3	147.65	147.73	151.42
P1-C1-N1-C2	-79.92	-81.85	-78.61
P2-C2-N1-C3	-147.65	-148.87	-151.44
P2-C2-N1-C1	79.92	80.66	78.59
R1-P1-C1-N1	169.63	164.48	167.24
R2-P1-C1-N1	-82.78	86.85	-84.29
R3-P2-C2-N1	-169.64	-162.71	-167.23
R4-P2-C2-N1	82.78	89.15	84.29

Table 3.40. The Mulliken charges for $[NiI_2(Me_2PCH_2)_2NMe]$, $[NiI_2(Cy_2PCH_2)_2NMe]$ and $[NiI_2(Ph_2PCH_2)_2NMe]$

	R		
	Me	**Cy**	**Ph**
Ni	-0.428	-0.534	-0.329
I1	-0.209	-0.204	-0.216
I2	-0.209	-0.205	-0.216
P1	0.734	0.746	0.705
P2	0.734	0.747	0.705
R1	-0.087	-0.035	-0.085
R2	-0.069	-0.035	-0.082
R3	-0.087	-0.038	-0.086
R4	-0.069	-0.036	-0.082
$N(me)(CH_2)_2$	-0.306	-0.401	-0.313

The optimized structures of the Palladium complexes $[PdI_2(Me_2PCH_2)_2NMe]$, $[PdI_2(Cy_2PCH_2)_2NMe]$, $[PdI_2(Ph_2PCH_2)_2NMe]$ complexes are shown in Figure 3.15. The calculated bond lengths, the bond angles, the dihedral angles and the Mulliken charges are shown in Table 3.41, Table 3.42, Table 3.43 and Table 3.44.

Table 3.41. The Mulliken charges for $[PdI_2(Me_2PCH_2)_2NMe]$, $[PdI_2(Cy_2PCH_2)_2NMe]$ and $[PdI_2(Ph_2PCH_2)_2NMe]$

	R		
	Me	**Cy**	**Ph**
Pd	-0.444	-0.570	-0.463
I1	-0.214	-0.210	-0.173
I2	-0.214	-0.211	-0.173
P1	0.732	0.771	0.716
P2	0.732	0.771	0.716
R1	-0.083	-0.019	-0.084
R2	-0.070	-0.020	-0.078
R3	-0.083	-0.040	-0.084
R4	-0.070	-0.041	-0.078
$N(Me)(CH_2)_2$	-0.286	-0.389	-0.302

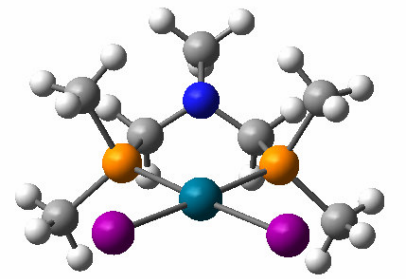

(a)

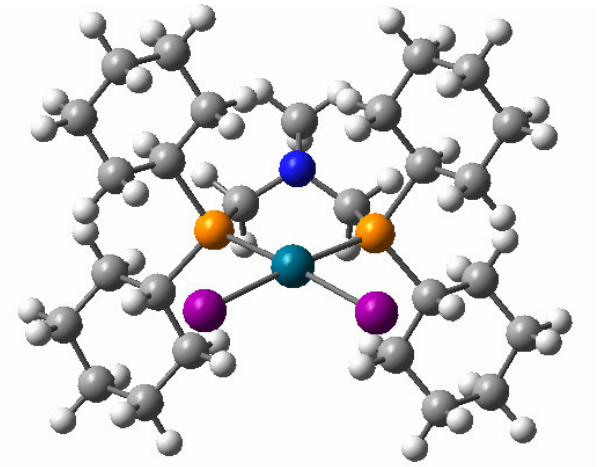

(b)

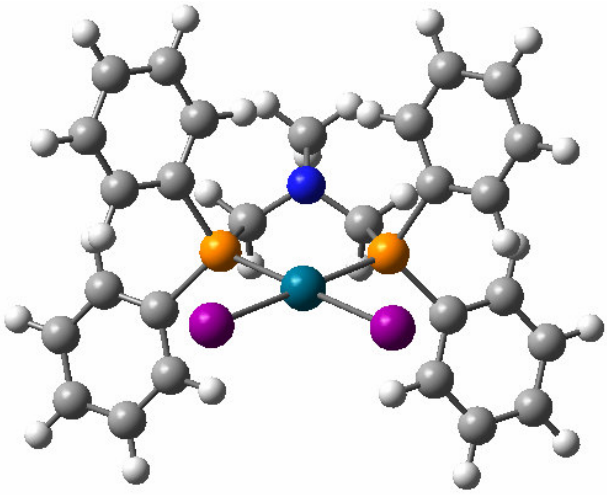

(c)

Figure 3.15. The structures of the complexes $[PdI_2(Me_2PCH_2)_2NMe]$ (a), $[PdI_2(Cy_2PCH_2)_2NMe]$ (b) and $[PdI_2(Ph_2PCH_2)_2NMe]$ (c)

Table 3.42. The calculated dihedral angles for $[PdI_2(Me_2PCH_2)_2NMe]$, $[PdI_2(Cy_2PCH_2)_2NMe]$ and $[PdI_2(Ph_2PCH_2)_2NMe]$

Dihedral	R		
	Me	Cy	Ph
Pd-P1-C1-N1	40.89	42.32	40.36
Pd-P2-C2-N1	-40.89	-40.74	-40.34
I1-Pd-P1-R1	53.50	52.45	57.53
I1-Pd-P1-R2	-68.62	-72.70	-67.88
I2-Pd-P2-R3	-53.50	-52.25	-57.50
I2-Pd-P2-R4	68.62	72.72	67.90
I1-Pd-P1-C1	173.30	168.01	173.38
I2-Pd-P2-C2	-173.30	168.07	-173.36
P1-C1-N1-C3	143.13	145.11	147.24
P1-C1-N1-C2	-82.98	-83.40	-81.72
P2-C2-N1-C3	-143.13	-146.11	-147.26
P2-C2-N1-C1	-82.98	82.37	81.71
R1-P1-C1-N1	169.22	164.31	166.72
R2-P1-C1-N1	-82.74	-86.49	-84.68
R3-P2-C2-N1	-169.22	-162.97	-166.72
R4-P2-C2-N1	82.74	87.93	84.68

For the palladium complexes Pd-P bond length shows the trend cy > ph > me. Pd-I bond length has the trend cy > me > ph which is also the trend for the R-P bond length. P-C bond length has the trend ph > cy > me. I-Pd-I angle and I-Pd-P angle are close to 90° forming a square planar geometry. The bite angle P-M-P is the largest for the cyclohexyl substituted complex with 94.20° and the smallest for the methyl substituted complex with 93.48°. Pd-P-C-N dihedral angles are about 40°.

The negative charge Pd has the trend cy > ph > me. The positive charge on P has the trend cy > me > ph. The negative charge on the $N(Me)(CH_2)_2$ fragment has the trend as cy > ph > me.

Table 3.43. The calculated angles for $[PdI_2(Me_2PCH_2)_2NMe]$, $[PdI_2(Cy_2PCH_2)_2NMe]$ and $[PdI_2(Ph_2PCH_2)_2NMe]$

Angle	R		
	Me	**Cy**	**Ph**
Pd-P1-C1	116.98	115.52	116.28
Pd-P2-C2	116.99	115.82	116.28
Pd-P1-R1	117.33	112.71	117.64
Pd-P1-R2	112.72	118.53	114.14
Pd-P2-R3	117.33	112.77	117.66
Pd-P2-R4	112.72	118.36	114.12
I1-Pd-P1	87.49	88.76	88.31
I2-Pd-P2	87.49	88.81	88.32
I1-Pd-I2	91.42	86.14	89.42
P1-Pd-P2	93.48	94.20	93.90
P1-C1-N1	113.45	114.62	115.03
C1-N1-C2	113.82	113.42	113.46
C1-N1-C3	114.31	113.54	113.31
C2-N1-C3	114.31	113.49	113.31
P2-C2-N1	113.45	114.76	115.03
R1-P1-C1	100.66	101.12	98.10
R2-P1-C1	102.22	100.50	102.27
R3-P2-C2	100.66	101.12	98.10
R4-P2-C2	102.22	100.35	102.27
R1-P1-R2	104.97	106.39	106.18
R3-P2-R4	104.97	106.33	106.17

Table 3.44 The calculated bond lengths for $[PdI_2(Me_2PCH_2)_2NMe]$, $[PdI_2(Cy_2PCH_2)_2NMe]$ and $[PdI_2(Ph_2PCH_2)_2NMe]$

Bond	**R**		
	Me	**Cy**	**Ph**
Pd-P1	2.405	2.429	2.423
Pd-P2	2.405	2.431	2.423
Pd-I1	2.717	2.733	2.714
Pd-I2	2.717	2.733	2.714
P1-C1	1.912	1.916	1.921
C1-N1	1.469	1.471	1.470
N1-C3	1.480	1.480	1.483
P2-C2	1.912	1.917	1.921
C2-N1	1.469	1.471	1.470
R1-P1	1.882	1.918	1.878
R2-P1	1.880	1.929	1.875
R3-P2	1.882	1.918	1.878
R4-P2	1.880	1.929	1.875

The optimized structures of the Platinum complexes $[PdI_2(Me_2PCH_2)_2NMe]$, $[PdI_2(Cy_2PCH_2)_2NMe]$, $[PdI_2(Ph_2PCH_2)_2NMe]$ are shown in Figure 3.16. The calculated bond lengths, bond angles, dihedral angles and the Mulliken charges are shown in Table 3.45, Table 3.46, Table 3.47 and Table 3.48.

Table 3.45. The calculated bond lengths for $[PtI_2(Me_2PCH_2)_2NMe]$, $[PtI_2(Cy_2PCH_2)_2NMe]$ and $[PtI_2(Ph_2PCH_2)_2NMe]$

Bond	**R**		
	Me	**Cy**	**Ph**
Pt-P1	2.377	2.396	2.387
Pt-P2	2.377	2.396	2.387
Pt-I1	2.738	2.752	2.734
Pt-I2	2.738	2.752	2.734
P1-C1	1.909	1.913	1.917
C1-N1	1.468	1.470	1.469
N1-C3	1.480	1.480	1.484
P2-C2	1.909	1.913	1.917
C2-N1	1.468	1.470	1.469
R1-P1	1.879	1.916	1.876
R2-P1	1.877	1.928	1.874
R3-P2	1.879	1.916	1.876
R4-P2	1.877	1.927	1.874

Table 3.46. The Mulliken charges for $[PtI_2(Me_2PCH_2)_2NMe]$, $[PtI_2(Cy_2PCH_2)_2NMe]$ and $[PtI_2(Ph_2PCH_2)_2NMe]$

	R		
	Me	**Cy**	**Ph**
Pt	-0.626	-0.718	-0.620
I1	-0.155	-0.154	-0.116
I2	-0.155	-0.154	-0.116
P1	0.716	0.732	0.680
P2	0.716	0.733	0.680
R1	-0.065	-0.015	-0.051
R2	-0.054	-0.019	-0.066
R3	-0.065	-0.017	-0.052
R4	-0.054	-0.020	-0.065
$N(Me)(CH_2)_2$	-0.275	-0.368	-0.277

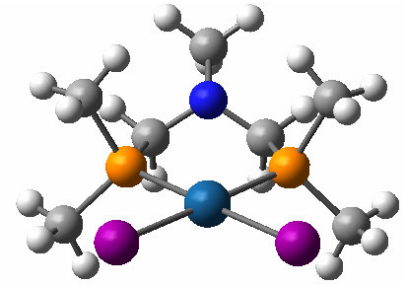

(a)

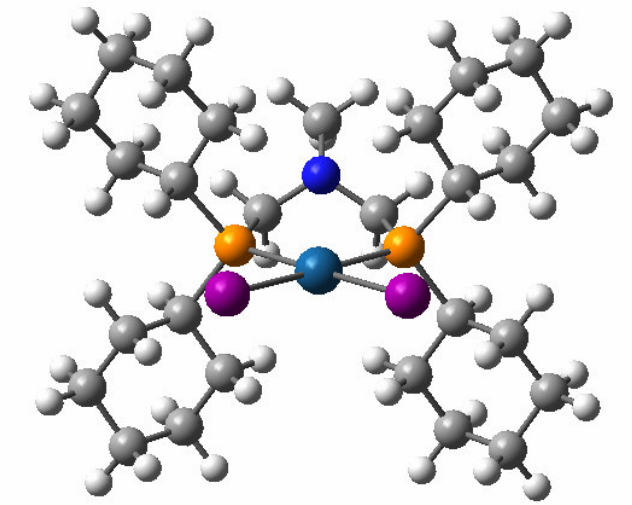

(b)

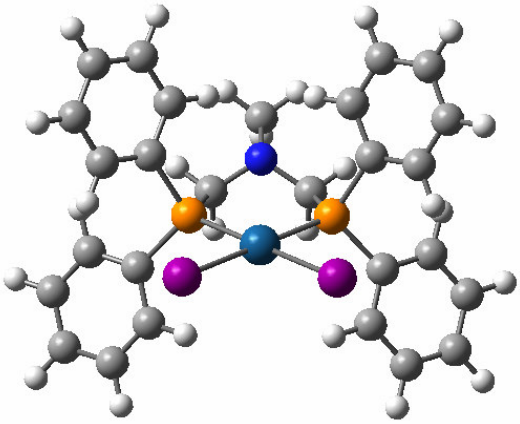

(c)

Figure 3.16. The structures of $[PtI_2(Me_2PCH_2)_2NMe]$ (a), $[PtI_2(Cy_2PCH_2)_2NMe]$ (b) and $[PtI_2(Ph_2PCH_2)_2NMe]$ (c)

Pt-P bond length shows the trend cy > ph > me. The Pt-I bond length has the trend cy > me > ph which is also the trend for the R-P bond length. P-C bond length has the trend ph > cy > me. I-Pt-I angle and I-Pt-P angle are again close to 90° indicating a square planar geometry. The bite angle P-M-P is the largest for the cyclohexyl substituted complex with 95.20° and the smallest for the methyl substituted complex with 94.60°. Pt-P-C-N dihedral angles are about 40° and symmetric for the methyl and phenyl substituted complexes.

The negative charge on Pt was has the trend cy > me > ph. The positive charge on P has the trend cy > me > ph. The negative charge on the $N(Me)(CH_2)_2$ fragment has the trend cy > ph > me

Table 3.47. The calculated dihedral angles for $[PtI_2(Me_2PCH_2)_2NMe]$, $[PtI_2(Cy_2PCH_2)_2NMe]$ and $[PtI_2(Ph_2PCH_2)_2NMe]$

Dihedral	**R**		
	Me	**Cy**	**Ph**
Pt-P1-C1-N1	41.07	41.84	40.60
Pt-P2-C2-N1	-41.07	-40.96	-40.61
I1-Pt-P1-R1	53.66	52.68	57.99
I1-Pt-P1-R2	-68.70	-72.44	-67.66
I2-Pt-P2-R3	-53.66	-52.33	-57.97
I2-Pt-P2-R4	68.70	72.67	67.67
I1-Pt-P1-C1	172.80	168.34	173.33
I2-Pt-P2-C2	-172.80	-168.21	-173.31
P1-C1-N1-C3	143.19	145.88	147.94
P1-C1-N1-C2	-82.84	-82.71	-81.38
P2-C2-N1-C3	-143.19	-146.44	-147.94
P2-C2-N1-C1	82.84	82.14	81.38
R1-P1-C1-N1	168.48	163.88	166.03
R2-P1-C1-N1	-82.74	-86.68	-84.72
R3-P2-C2-N1	168.48	163.22	-166.03
R4-P2-C2-N1	82.74	87.40	84.71

Table 3.48. The calculated angles for the $[PtI_2(Me_2PCH_2)_2NMe]$, $[PtI_2(Cy_2PCH_2)_2NMe]$ and $[PtI_2(Ph_2PCH_2)_2NMe]$

Angle	R		
	Me	**Cy**	**Ph**
Pt-P1-C1	116.46	115.35	115.97
Pt-P2-C2	116.46	115.53	115.97
Pt-P1-R1	116.73	112.74	116.87
Pt-P1-R2	112.79	118.25	114.37
Pt-P2-R3	116.73	112.83	116.87
Pt-P2-R4	112.79	118.09	114.37
I1-Pt-P1	87.58	88.83	88.19
I2-Pt-P2	87.58	88.87	88.20
I1-Pt-I2	90.14	87.03	88.61
P1-Pt-P2	94.60	95.20	94.94
P1-C1-N1	113.52	114.67	115.02
C1-N1-C2	113.64	113.25	113.13
C1-N1-C3	114.42	113.56	113.29
C2-N1-C3	114.42	113.56	113.29
P2-C2-N1	113.51	114.76	115.02
R1-P1-C1	100.90	101.28	98.35
R2-P1-C1	102.79	100.71	102.51
R3-P2-C2	100.90	101.30	98.35
R4-P2-C2	102.79	100.64	102.51
R1-P1-R2	105.46	107.02	106.68
R3-P2-R4	105.46	107.02	106.68

3.4.2. The Comparison of the Iodine Complexes of the Ni, Pd and Pt derivatives of the $(Me_2PCH_2)_2NMe$, $(Cy_2PCH_2)_2NMe$ and $(Ph_2PCH_2)_2NMe$

Nickel, Palladium and Platinum complexes all have the same following trends for different substituents:

- M-P → cy > ph > me
- M-I → cy > me > ph
- P-C → ph > cy > me
- R-P → cy > me > ph

The methyl, cyclohexyl and the phenyl complexes all have the same following trends for different metals:

- M-P → Pd > Pt > Ni
- M-I → Pt > Pd > Ni
- P-C → Ni > Pd > Pt
- R-P → Ni > Pd > Pt

Table 3.49.The calculated bite angles for the I complexes

	R		
	Cy	**Ph**	**Me**
Ni	95.39	94.05	93.51
Pd	94.20	93.90	93.48
Pt	95.20	94.94	94.60

The cyclohexyl substituted complexes have larger bite angles compared to their methyl and phenyl substituted analogues.

The charges of the I complexes give the following trends:

- The negative charge on the M atom → cy > me > ph for Ni and Pt complexes,
  cy > ph > me for the Pd complexes
- The positive charge on the P atom → cy > me > ph
- The negative charge on the R groups → me ≈ ph > cy
- The negative charge on the $N(Me)(CH_2)_2$ fragment → cy > ph > me

The methyl, cyclohexyl and the phenyl complexes all have the same following trends for different metals:

- The negative charge on the M atom → Pt > Pd > Ni
- The positive charge on the P atom → Pd > Ni > Pt
- The negative charge on the R groups → Ni > Pd > Pt
- The negative charge on the $N(Me)(CH_2)_2$ fragment → Ni > Pd > Pt

Upon complexation, the positive charge on the P atom increases with the trend cy > me > ph; cyclohexyl substituted complex having the most increase.

3.5. The Comparison of the Chlorine, Bromine and Iodine Complexes of the Ni, Pd and Pt derivatives of the $(Me_2PCH_2)_2NMe$, $(Cy_2PCH_2)_2NMe$ and $(Ph_2PCH_2)_2NMe$

Each Cl, Br and I series of each M all have the same following trends:

- M-X → cy > me > ph
- M-P → cy > ph > me
- P-C → ph > cy > me
- R-P → cy > me > ph

The R-P distances for phenyl complexes are shorter than methyl and cyclohexyl substituted complexes. This is due to the π-bonding between the P atom and the phenyl groups.

The methyl, cyclohexyl and the phenyl complexes all have the same following trends for different metals:

- M-X bond → Pt > Pd > Ni
- M-P bond → Pd > Pt > Ni
- P-C bond → Ni > Pd > Pt
- R-P bond → Ni > Pd > Pt

M-P bonds are longest for Pd decreasing in the order Pd > Pt > Ni. This unexpected trend urged us to carry out calculations for $(CO)_2PdCl_2$ and $(CO)_2PtCl_2$ complexes to check if the same trend would be observed and we found Pd-CO bond distances(1.957 Å) to be longer than Pt-CO (1.911 Å). A similar case for Pt being smaller than Pd is reported for

their methyl-based covalent radii [35]. Also, Au is reported to be smaller than Ag in numerous cases [36-40].

Upon changing the halogen atoms, the following trends are observed for each M series and each R series:

- M-X bond → I > Br > Cl
- M-P bond → I > Br > Cl
- P-C bond → I > Br > Cl
- R-P bond → I > Br > Cl

X-M-X angle has the following trends:

- me > ph > cy ; for each of M and X series
- Pd ≈ Ni > Pt ; for each oh X and R series
- Cl > Br > I ; for each of M and R series

The bite angle P-M-P is always the largest for the cyclohexyl substituted complexes compared to their phenyl and methyl analogues. The bite angle is also the largest for the Pt complexes compared to the Ni and Pd analogs. For each M series and each R groups it has the trend Cl > Br > I. X-M-X and P-M-P are opposite angles in the square planar conformation around the metal atom and have the same trends. When the M-X distance is smallest the two halogens stay apart from each other by the presence of the largest X-M-X angle.

R-P-R angles are all about 160° and have trend ph > cy > me for all complexes. This result is expected because the phenyl and the cyclohexyl groups are bigger than the methyl group so that they will stay apart from each other because of steric crowding.

M-P-C-N dihedral angle for the series of each metal atom has the trend I > Br > Cl for the methyl substituted complexes. Cyclohexyl substituted complexes have different M-P1-C1-N1 and M-P2-C2-N1 dihedrals whereas methyl and phenyl substituted complexes have symmetric M-P-C-N angles. For the series of each halogen complexes the M-P-C-N dihedral angle has the trends as ph > cy > me and Pt > Pd > Ni.

The charges give the following trends:

- The negative charge on the metal atoms: I > Br > Cl

As the electronegativity increases in the order I < Br < Cl the chlorine atoms have more charge compared to the bromine and iodine atoms. Also, each series of the Cl, Br and I complexes of the same metal have the charges on the R groups and the C-N-C fragment very close to each other. This shows that the halogens pull the electrons mainly from the M atom so that the trend of the charges on the M atoms (largest for I, smallest for Cl) is the reverse of the electronegativity trend.

- The positive charge on the phosphorus atoms: Cl > Br > I

This results a decrease in the negative charge on the metal atoms for the chlorine complexes. So, there is an electron flow from the phosphorus atoms to the metal atom, which makes M-P bonds shorter for the chlorine complexes compared to the bromine and the iodine complexes.

The negative charge on the M atom is always bigger for cyclohexyl complexes compared to their phenyl and methyl complexes.

- The positive charge on the P atom : cy > me > ph

- The negative charge on the R groups : me ≈ ph > cy

- The negative charge on the $N(Me)(CH_2)_2$ fragment : cy > ph > me

The methyl, cyclohexyl and the phenyl complexes all have the same following trends for different metals:

- The negative charge on the M atom : Pt > Pd > Ni
- The positive charge on the P atom : Pd > Ni > Pt
- The negative charge on the R groups : Ni > Pd > Pt
- The negative charge on the $N(Me)(CH_2)_2$ fragment : Ni > Pd > Pt

Upon complexation P-C and R-P bond lengths decrease. This decrease is the biggest for the Cl complexes and the smallest for the I complexes. N-C distances also decrease. This decrease is the biggest for the I complexes and the methyl substituted complexes. N-C(Me) bond lengths increase but in small amounts. This increase is the largest for the Ph complexes and independent of the halogen and the metal atoms. As R-P and P-C distances decrease, N-C(Me) bond lengths increase, the total charge of the C-N-C fragment decreases. As the charge on the C-N-C fragment decreases, the charges flows through the P atoms, resulting a decrease in the positive charge of the P atoms.

The charges on the R groups decrease. This decrease is the largest for the cy substituents and about equal for the me and ph substituents.

Upon complexation the decrease in the R-P distances would get the two R groups on the same P atom closer to each other but the R-P-R angle increase so that they stay apart from each other. The R-P distances for the Ph substituted complexes are smaller then the methyl and cyclohexyl substituted complexes thus having the larger R-P-R angles.

The positive charge on the P atoms increase in the order ph < cy < me for Ni and Pt complexes and ph < me < cy for Pd complexes. For the same metal atom and the same substituent on the P atom, this increase has the trend I < Br < Cl. Cl, being more electronegative then Br and I, attracts electrons more. As this electron flow towards the

halogen increases, the positive charge on the P atom increases. This explains the more positive charges on the P atoms for the Cl complexes.

The negative charge on the C-N-C fragment decreases. This decrease is the largest for the methyl complexes having the trend me > cy > ph and is not affected much by changing the halogen atoms.

3.6. $[PdCl_2(Ph_2PCH_2)_2NPh]$ Complex: The Effect of Substituent on the Nitrogen Atom of the Ligand

Up to now all complexes include a methyl group on the nitrogen atom of the ligand. When those complexes are to be used as catalysts for example in a heterogeneous catalysis, they are bounded to a solid support from the N atom. If the conjunction point of the solid support involves a bulky group, it may affect all the geometrical parameters and charges of the complex molecule.

To examine the effect of substituent bonded to N atom on the complex structure, the methyl group on the N atom was replaced with a phenyl group. First conformer search was done for the Ni derivative by using PM3 method. The lowest energy conformer was chosen. The coordinates of this conformer was taken, the Ni atom was replaced with the Pd atom and the final structure of $[PdCl_2(Ph_2PCH_2)_2NPh]$ was optimized with the DFT method.

The final structure of $[PdCl_2(Ph_2PCH_2)_2NPh]$ is shown in Figure 3.17. The calculated bond lengths, angles, dihedral angles and charges of the complexes $[PdCl_2(Ph_2PCH_2)_2NMe]$ and $[PdCl_2(Ph_2PCH_2)_2NPh]$ were shown together in Table 3.50, Table 3.51, Table 3.52 and Table 3.53 to make comparisons.

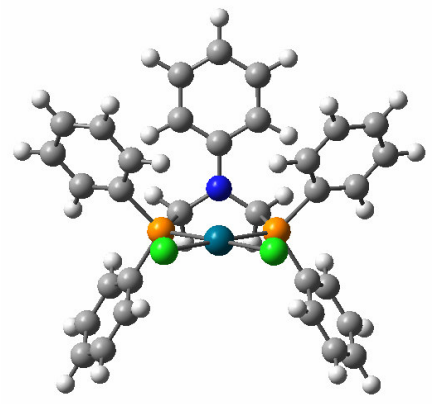

Figure 3.17. The structure of $[PdCl_2(Ph_2PCH_2)_2NPh]$

The structure of $[PdCl_2(Ph_2PCH_2)_2NPh]$ is interesting in the orientations of the Ph groups on the N atom and the Phosphorus atoms. The two phenyl groups on different P atoms and the phenyl group on the N form a cage like structure.

Table 3.50. The calculated bond lengths for $[PdCl_2(Ph_2PCH_2)_2NMe]$ and $[PdCl_2(Ph_2PCH_2)_2NPh]$

Bond	**N-Me**	**N-Ph**
Pd-P1	2.379	2.406
Pd-P2	2.379	2.405
Pd-Cl1	2.419	2.417
Pd-Cl2	2.419	2.417
P1-C1	1.915	1.940
C1-N1	1.472	1.452
N1-C3	1.484	1.422
P2-C2	1.915	1.940
C2-N1	1.472	1.452
R1-P1	1.875	1.882
R2-P1	1.871	1.878
R3-P2	1.875	1.882
R4-P2	1.871	1.879

Table 3.51. The calculated angles for $[PdCl_2(Ph_2PCH_2)_2NMe]$ and $[PdCl_2(Ph_2PCH_2)_2NPh]$

Angle	N-Me	N-Ph
Pd-P1-C1	116.07	113.48
Pd-P2-C2	116.07	113.52
Pd-P1-R1	117.02	115.16
Pd-P1-R2	112.93	115.14
Pd-P2-R3	117.02	115.22
Pd-P2-R4	112.93	115.03
Cl1-Pd-P1	85.71	85.92
Cl2-Pd-P2	85.71	85.87
Cl1-Pd-Cl2	93.61	90.83
P1-Pd-P2	94.93	97.38
P1-C1-N1	115.11	114.71
C1-N1-C2	113.80	114.77
C1-N1-C3	112.90	122.60
C2-N1-C3	112.90	122.60
P2-C2-N1	115.11	114.70
R1-P1-C1	99.15	101.63
R2-P1-C1	103.72	103.38
R3-P2-C2	99.15	101.61
R4-P2-C2	103.72	103.36

Table 3.52. The calculated dihedral angles for $[PdCl_2(Ph_2PCH_2)_2NMe]$ and $[PdCl_2(Ph_2PCH_2)_2NPh]$

Dihedral	N-Me	N-Ph
Pd-P1-C1-N1	41.89	29.21
Pd-P2-C2-N1	-41.89	-29.10
Cl1-Pd-P1-R1	53.69	70.27
Cl1-Pd-P1-R2	-70.09	-54.34
Cl2-Pd-P2-R3	-53.70	-70.19
Cl2-Pd-P2-R4	70.08	54.46
Cl1-Pd-P1-C1	170.33	-173.18
Cl2-Pd-P2-C2	-170.33	173.22
P1-C1-N1-C3	149.38	94.06
P1-C1-N1-C2	-80.24	-84.05
P2-C2-N1-C3	-149.38	-94.14
P2-C2-N1-C1	80.24	83.97
R1-P1-C1-N1	168.13	153.45
R2-P1-C1-N1	-82.58	-96.20
R3-P2-C2-N1	-168.12	-153.42
R4-P2-C2-N1	82.59	96.18

Table 3.53. The Mulliken Charges for $[PdCl_2(Ph_2PCH_2)_2NMe]$ and $[PdCl_2(Ph_2PCH_2)_2NPh]$

	N-Me	N-Ph
Pd	-0.313	-0.347
Cl1	-0.286	-0.273
Cl2	-0.286	-0.273
P1	0.739	0.701
P2	0.739	0.701
R1	-0.073	-0.071
R2	-0.067	-0.034
R3	-0.073	-0.071
R4	-0.067	-0.034
$N(Me)(CH_2)_2$	-0.310	-0.298

Upon changing the methyl group on the N atom with a phenyl group Pd-P, P-C and R-P bond lengths increase, the Pd-Cl remain about the same, whereas, C1-N1, C2-N1 and especially N1-C3 bond lengths decrease significantly. This can be attributed to the Phenyl ring on the Nitrogen atom which can make resonance with N atom thus making an electron-withdrawing effect. The π-bond formation between the N atom and the phenyl ring on it is observed on HOMO(-15) (Figure a) and HOMO(-19) (Figure b) of $[PdCl_2(Ph_2PCH_2)_2NPh]$.

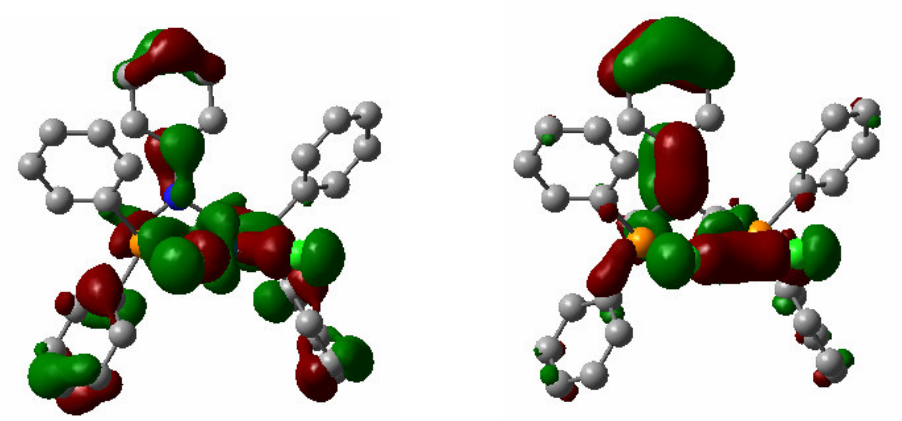

a) (b)

Figure 3.18. HOMO(-15) (a) and HOMO(-19) (b) of $[PdCl_2(Ph_2PCH_2)_2NPh]$

The bite angle P-Pd-P increases about 2° becoming 97.38°, which is the largest of all complexes. Changing the methyl group with phenyl group affects the Pd-P1-C1-N1 and Pd-P2-C2-N1 dihedral angles most. They shrink from about 42° to 29°.

The charges are also affected upon changing the methyl group on the N atom with a phenyl group. All the charges decrease from $[PdCl_2(Ph_2PCH_2)_2NMe]$ to $[PdCl_2(Ph_2PCH_2)_2NPh]$ except the negative charge on the Pd atom which increases. N atom, together with the withdrawing effect of the phenyl group attracts electron more, making the C1 and C2 carbon less electronegative thus decreasing the electronegativity difference between P an C atoms. This results in a less positive charge on the P atoms and an increase in the charge of the Pd atom.

3.7. $[PtCl_2(Ph_2PCH_2)_2CH_2]$ Complex: The Effect of Nitrogen Atom of the Ligand

There are several reasons that aminomethylphosphine ligands are chosen instead of their C derivatives. The amino functionality makes their synthesis easier and they can easily be attached to other groups by making use of this amino functionality [8-10,13]. But there are also structural differences between these complexes which may lead to different reactivities. To examine these structural differences $[PtCl_2(Ph_2PCH_2)_2CH_2]$ complex was optimized by DFT method to compare with the $[PtCl_2(Ph_2PCH_2)_2NMe]$ complex. The optimized structure of $[PtCl_2(Ph_2PCH_2)_2CH_2]$ is shown in Figure 3.19. The calculated bond lengths, angles, dihedral angles and Mulliken charges for both species are shown in Table 3.54, Table 3.55, Table 3.56 and Table 3.57.

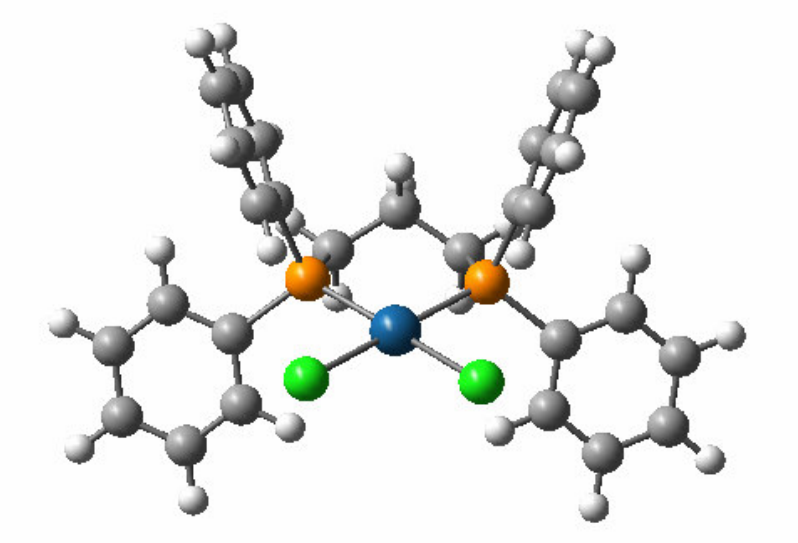

Figure 3.19. The optimized structure of $[PtCl_2(Ph_2PCH_2)_2CH_2]$

Table 3.54. The calculated bond lengths of $[PtCl_2(Ph_2PCH_2)_2CH_2]$

Bond	N-Ph	C-Ph
Pt-P1	2.352	2.365
Pt-P2	2.352	2.365
Pt-Cl1	2.443	2.443
Pt-Cl2	2.443	2.443
P1-C1	1.910	1.894
C1-C3	1.472	1.545
P2-C2	1.910	1.894
C2-C3	1.472	1.545
R1-P1	1.873	1.876
R2-P1	1.870	1.878
R3-P2	1.873	1.876
R4-P3	1.870	1.878

Table 3.55. The Mulliken charges of $[PtCl_2(Ph_2PCH_2)_2CH_2]$

	N-Ph	C-Ph
Pt	-0.440	-0.473
X1	-0.237	-0.233
X2	-0.237	-0.233
P1	0.694	0.639
P2	0.694	0.639
R1	-0.030	-0.008
R2	-0.063	-0.062
R3	-0.030	-0.008
R4	-0.063	-0.062
$N(Me)(CH_2)_2$/ $CH_2(CH_2)_2$	-0.283	-0.194

Table 3.56. The calculated angles of $[PtCl_2(Ph_2PCH_2)_2CH_2]$

Angle	N-Ph	C-Ph
Pt-P1-C1	115.49	115.18
Pt-P2-C2	115.49	115.18
Pt-P1-R1	116.37	116.36
Pt-P1-R2	113.15	111.99
Pt-P2-R3	116.38	116.36
Pt-P2-R4	113.15	111.99
X1-Pt-P1	86.74	87.20
X2-Pt-P2	86.75	87.20
X1-Pt-X2	91.00	89.46
P1-Pt-P2	95.43	96.02
P1-C1-C3	115.47	116.06
C1-C3-C2	113.81	113.37
P2-C2-C3	115.48	116.06
R1-P1-C1	99.11	100.21
R2-P1-C1	104.68	105.29
R3-P2-C2	99.11	100.21
R4-P2-C2	104.67	105.29

Table 3.57. The calculated dihedral angles of $[PtCl_2(Ph_2PCH_2)_2CH_2]$

Dihedral	N-Ph	C-Ph
Pt-P1-N1(C1)-C3	44.83	48.08
Pt-P2-N2(C1)-C3	-44.83	-48.08
X1-Pt-P1-R1	50.60	44.14
X1-Pt-P1-R2	-73.20	-78.75
X2-Pt-P2-R3	-50.60	-44.14
X2-Pt-P2-R4	73.20	78.75
X1-Pt-P1-C1	166.20	160.99
X2-Pt-P2-C2	-166.20	-160.99
P1-C1-C3-C2	-78.92	-75.87
P2-C2-C3-C1	78.92	75.87
R1-P1-C1-C3	169.91	173.76
R2-P1-C1-C3	-80.27	-75.79
R3-P2-C2-C3	169.92	-173.76
R4-P2-C2-C3	80.28	-75.79

Changing C atom on the backbone of the ligand with N atom does not result in significant changes both in the electronic and geometrical parameters of the complexes. The bond lengths and angles are almost the same. The dihedral angle Pt-P-C-N-(C) shrinks about 3° and the negative charge on the Pt atom, with a small decrease, remains almost the same.

3.8. The Rhodium Derivatives [$RhCl_2(Me_2PCH_2)_2NMe$] and [$RhI_2(Me_2PCH_2)_2NMe$]

After investigating the changes upon changing the metal atom down the group on the periodic table, the effect of Rh atom, which lies on the same period with Pd atom, was examined. For this purpose, the structures of Rh derivatives of the methyl substituted Cl and I complexes were optimized. The structures of Rh complexes were obtained by taking the coordinates of the optimized structure of the Pd analogues, replacing Pd with Rh atom and reoptimizing with DFT method. The optimized structures of the [$RhCl_2(Me_2PCH_2)_2CHMe$] and [$RhI_2(Me_2PCH_2)_2CHMe$] are shown in Figure 3.20. The calculated bond lengths,

angles, dihedral angles and the Mulliken charges are shown in Table 3.58, Table 3.59, Table 3.60 and Table 3.61.

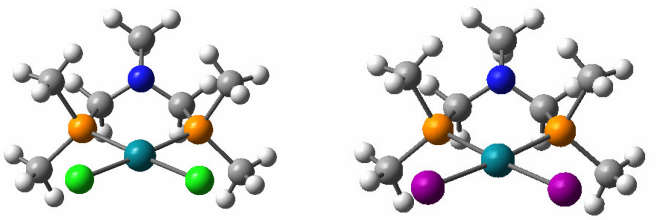

(a) (b)

Figure 3.20. The optimized structures of $[RhCl_2(Me_2PCH_2)_2NMe]$ and $[RhI_2(Me_2PCH_2)_2NMe]$

Table 3.58. The calculated bond lengths for the structures of $[RhCl_2(Me_2PCH_2)_2NMe]$ and $[RhI_2(Me_2PCH_2)_2NMe]$

Bond	**X**	
	Cl	**I**
Rh-P1	2.389	2.431
Rh-P2	2.389	2.432
Rh-X1	2.447	2.700
Rh-X2	2.447	2.700
P1-C1	1.910	1.910
C1-N1	1.472	1.469
N1-C3	1.480	1.480
P2-C2	1.910	1.910
C2-N1	1.472	1.469
R1-P1	1.879	1.885
R2-P1	1.878	1.883
R3-P2	1.879	1.885
R4-P2	1.878	1.883

Table 3.59. The calculated angles for the structures of $[RhCl_2(Me_2PCH_2)_2NMe]$ and $[RhI_2(Me_2PCH_2)_2NMe]$

Angle	X	
	Cl	I
Rh-P1-C1	116.42	118.47
Rh-P2-C2	116.42	118.47
Rh-P1-R1	115.82	117.24
Rh-P1-R2	112.07	112.95
Rh-P2-R3	115.82	117.24
Rh-P2-R4	112.07	112.95
X1-Rh-P1	84.36	88.39
X2-Rh-P2	84.36	88.38
X1-Rh-X2	96.35	92.04
P1-Rh-P2	94.87	90.98
P1-C1-N1	112.93	113.56
C1-N1-C2	114.30	113.58
C1-N1-C3	114.26	114.14
C2-N1-C3	114.26	114.14
P2-C2-N1	112.93	113.56
R1-P1-C1	102.84	100.07
R2-P1-C1	103.52	101.81
R3-P2-C2	102.84	100.07
R4-P2-C2	103.52	101.81

Table 3.60. The calculated dihedral angles for the structures of $[RhCl_2(Me_2PCH_2)_2NMe]$ and $[RhI_2(Me_2PCH_2)_2NMe]$

Dihedral	X	
	Cl	I
Rh-P1-C1-N1	38.97	42.42
Rh-P2-C2-N1	-38.97	-42.41
X1-Rh-P1-R1	53.99	51.96
X1-Rh-P1-R2	-66.05	-69.01
X2-Rh-P2-R3	53.99	-51.95
X2-Rh-P2-R4	66.05	69.01
X1-Rh-P1-C1	175.06	172.15
X2-Rh-P2-C2	-175.06	-172.14
P1-C1-N1-C3	141.89	144.82
P1-C1-N1-C2	-83.84	-81.97
P2-C2-N1-C3	-141.89	-144.82
P2-C2-N1-C1	83.84	81.97
R1-P1-C1-N1	166.71	171.11
R2-P1-C1-N1	-84.46	-82.09
R3-P2-C2-N1	-166.71	-171.10
R4-P2-C2-N1	84.46	82.10

Table 3.61. The Mulliken charges for the structures of $[RhCl_2(Me_2PCH_2)_2NMe]$ and $[RhI_2(Me_2PCH_2)_2NMe]$

	X	
	Cl	I
Rh	-0.173	-0.405
X1	-0.333	-0.180
X2	-0.333	-0.180
P1	0.719	0.695
P2	0.719	0.695
R1	-0.083	-0.090
R2	-0.073	-0.078
R3	-0.083	-0.090
R4	-0.073	-0.078
$N(Me)(CH_2)_2$	-0.280	-0.288

For methyl substituted complexes, Rh-P, Rh-X and R-P distances are longer for the iodine complexes compared to the chlorine complexes. X-Rh-X and P-Rh-P angles are larger for

the chlorine complexes then the iodine complex. M-P-C-N angles are symmetric for both chlorine and the iodine complexes and increases from chlorine complexes to iodine complexes. The negative charge on the Rh atom is bigger for the iodine complexes than the chlorine complexes. The charge on the phosphorus atom is bigger for the chlorine complexes than the iodine complexes.

The chlorine and iodine substituted $[RhX_2(Me_2PCH_2)_2NMe]$ complexes have slightly longer M-P, M-X and R-P bond lengths compared to the Pd derivatives. Changing the metal atom from Pd to Rh decreases the X-M-X angle for the chlorine complexes whereas increases it for the iodine complexes. The bite angle also decreases from Pd to Rh for both chlorine and iodine complexes. M-P-C-N angle decreases for the chlorine complexes whereas increases for the iodine complex. The charge on the Rh atom is smaller then the charge on the Pd for the chlorine complexes whereas it is bigger for the iodine complexes.

3.9. The Transition State Structure of the Ethylene Insertion Step of the Hydrogenation Reaction of Ethylene: $[PtH(et)(Me_2PCH_2)_2NMe]$ and $[PtH(et)(Ph_2PCH_2)_2NMe]$

The transition state structures of the ethylene insertion step of the hydrogenation reaction of ethylene, $[PtH(et)(Me_2PCH_2)_2NMe]$ and $[PtH(et)(Ph_2PCH_2)_2NMe]$, were obtained by making use of the B3LYP/LANL2DZ basis set. The transition state structures $[PtH(et)(Me_2PCH_2)_2NMe]$ and $[PtH(et)(Ph_2PCH_2)_2NMe]$ were verified with the one and only one negative frequency for each structure -653.30 cm^{-1} and -675.38cm^{-1} respectively. Both frequencies correspond to the stretching which represents the approach of the ethylene and the hydrogen atom each other. The transition state structures of $[PtH(et)(Me_2PCH_2)_2NMe]$ and $[PtH(et)(Ph_2PCH_2)_2NMe]$ are shown on Figure 3.21. The calculated bond lengths, bond angles, dihedral angles and Mulliken charges are shown on Table 3.62, Table 3.63, Table 3.64 and Table 3.65.

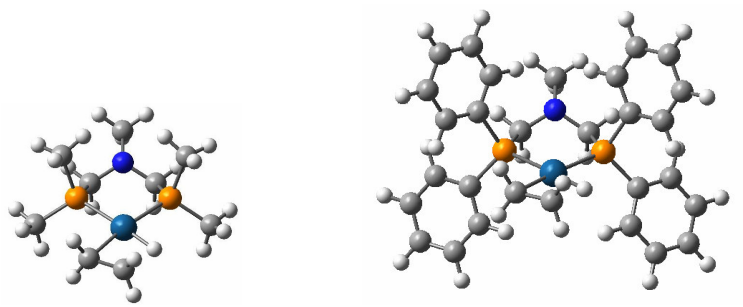

(a) (b)

Figure 3.21. The transition state structures of [PtH(et)(Me_2PCH_2)$_2$NMe] (a) and [PtH(et)(Ph_2PCH_2)$_2$NMe] (b)

Table 3.62. The bond lengths for the transition state structures [PtH(et)(Me_2PCH_2)$_2$NMe] and [PtH(et)(Ph_2PCH_2)$_2$NMe]

Bond	**R**	
	Me	**Ph**
Pt-P1	2.409	2.405
Pt-P2	2.411	2.405
Pt-H*	1.667	1.670
Pt-C2*	2.179	2.178
C1*-H*	1.609	1.602
C1*-C2*	1.442	1.443
P1-C1	1.909	1.916
C1-N1	1.467	1.470
N1-C3	1.484	1.487
P2-C2	1.910	1.916
C2-N1	1.467	1.469
R1-P1	1.879	1.869
R2-P1	1.877	1.873
R3-P2	1.879	1.869
R4-P2	1.877	1.871

Table 3.63. The angles for the transition state structures [PtH(et)($Me_2PCH_2)_2$NMe] and [PtH(et)($Ph_2PCH_2)_2$NMe]

Angle	R	
	Me	**Ph**
Pt-P1-C1	113.56	114.93
Pt-P2-C2	113.16	115.12
Pt-P1-R1	115.85	115.60
Pt-P1-R2	114.07	112.41
Pt-P2-R3	116.18	114.80
Pt-P2-R4	113.92	112.13
H*-Pt-P1	89.87	89.47
C2*-Pt-P2	95.68	94.08
H*-Pt-C2*	80.73	80.53
Pt-C2*-C1*	77.25	77.19
C2*-C1*-H*	111.28	111.43
C1*-H*-Pt	90.74	90.84
P1-Pt-P2	93.73	95.86
P1-C1-N1	111.92	114.16
C1-N1-C2	115.02	114.12
C1-N1-C3	115.20	113.67
C2-N1-C3	115.14	113.68
P2-C2-N1	111.86	114.29
R1-P1-C1	103.37	101.76
R2-P1-C1	103.46	104.32
R3-P2-C2	103.63	101.72
R4-P2-C2	103.40	105.00

Table 3.64. The dihedral angles for the transition state structures [PtH(et)($Me_2PCH_2)_2$NMe] and [PtH(et)($Ph_2PCH_2)_2$NMe]

Dihedral	**R**	
	Me	**Ph**
Pt-P1-C1-N1	51.71	40.04
Pt-P2-C2-N1	-52.68	-39.11
H*-Pt-P1-R1	34.64	55.38
H*-Pt-P1-R2	-87.71	-67.34
C2*-Pt-P2-R3	-33.76	-58.72
C2*-Pt-P2-R4	88.78	63.70
H*-Pt-P1-C1	154.08	173.54
C2*-Pt-P2-C2	-153.49	-176.36
C1*-C2*-Pt-P2	179.99	178.25
P1-C1-N1-C3	137.57	143.65
P1-C1-N1-C2	-84.89	-83.78
P2-C2-N1-C3	-136.85	-144.24
P2-C2-N1-C1	85.58	83.18
R1-P1-C1-N1	178.05	165.73
R2-P1-C1-N1	-72.47	-83.51
R3-P2-C2-N1	-179.37	-163.90
R4-P2-C2-N1	71.04	84.69

Table 3.65. The Mulliken charges for the transition state structures [PtH(et)($Me_2PCH_2)_2$NMe] and [PtH(et)($Ph_2PCH_2)_2$NMe]

	Me	**Ph**
Pt	-0.424	-0.432
H*	0.138	0.161
C2*	-0.467	-0.450
C1*	-0.464	-0.469
Et	0.195	0.216
P1	0.686	0.675
P2	0.708	0.718
R1	-0.046	-0.026
R2	-0.036	-0.036
R3	-0.056	-0.032
R4	-0.036	-0.054
N(Me)($CH_2)_2$	-0.127	-0.185

The Pt-P distance is longer for the methyl substituted TS than the phenyl substituted TS.

H*-Pt-C2* angle is larger for the methyl substituted TS whereas bite angle P-Pt-P is larger for the phenyl substituted TS. Pt-P-C-N angle is larger for the methyl substituted TS then the phenyl substituted TS. The charge on the Pt atom increases from the methyl substituted TS to the phenyl substituted TS.

When [PtH(et)(Me_2PCH_2)$_2$NMe] and [PtH(et)(Ph_2PCH_2)$_2$NMe] transition state structures are compared with the Cl, Br and I substituted [PtX_2(Me_2PCH_2)$_2$NMe] and [PtX_2(Ph_2PCH_2)$_2$NMe] complexes generally the bond lengths on the ligand for the transition state structures are longer than their Cl, Br and I complex derivatives. For the methyl substituted transition state the bite angle is smaller whereas for the phenyl substituted transition state the bite angle is larger compared to their complex derivatives. Pt-P-C-N dihedral angle is much larger for the methyl substituted TS than its analogues whereas it decreases for the phenyl substituted transition state compared to their halogen complexes.

All the charges for the transition state structures PtH(et)(Me_2PCH_2)$_2$NMe] and [PtH(et)(Ph_2PCH_2)$_2$NMe] are more than their Pt complex derivatives of the methyl and phenyl substituted ligands with halogen atoms being Cl, Br and I.

4. CONCLUSION

Significant changes both in the electronic character and the geometry of the complexes occur upon changing the metal atom, the halogen atoms and the substituents on the phosphorus atoms.

When the halogen atom and the metal atom are fixed cyclohexyl substituted complexes which include more electronegative C atom being bonded to the less electronegative P atom give longer bond lengths whereas, phenyl substituted complexes give smaller bond lengths. This is attributed to the π-bond observed between the P atom and the phenyl ring. The methyl substituted complexes also have longer R-P bond lengths than cyclohexyl groups which can be attributed to the hyperconjugation between the methyl group and the P atom.

Upon fixing the metal atom and the R substituents on the phosphorus atoms, the halogens also have significant effects on the electronic character and the geometry of the complexes. All the bond lengths increase in the order as Cl < Br < I.

The M-P bond length is mostly affected by the metal atom. Interestingly, M-P bond lengths for Pd complexes are found to be longer than the Pt complexes. Similar cases were reported on literature, specificaly for M-phosphine bonds [41].

Larger bite angles (P-M-P) are obtained when the substituent on the P atoms is cyclohexyl whereas smaller bite angles are obtained with the methyl groups. This can be attributed to the bulkiness of the cyclohexyl groups. Even though the bite angles are larger for the cyclohexyl groups, the two cyclohexyl groups on different P atoms are close to each other (2.4 Å) compared to the phenyl groups (2.7 Å). The bite angles are also the largest when the metal atom is Pt. The bite angles range between 86.14° and 97.38°. Literature contains examples [16] in which a certain bite angle is the optimum for a specific reaction. This means that, for a specific reaction, in which these complexes are to be used as catalysts, one can have choice of bite angles between 86.14° and 97.38°.

To obtain larger M-P-C-N dihedral angles phenyl substituted complexes with metal atoms being Pt must be used whereas smaller M-P-C-N dihedral angles are obtained with methyl substituted Ni complexes. All of M-P-C-N dihedral angles are about 40° and have small range, which may be regarded as a sign for their rigidity. Also, these complexes being rigid because of their six-memebered ring formation (M-P-C-N-C-P) can be selective for different products or reaction pathways.

Referring to the literature, the information above can be used to predict a better catalyst. In that sense, the Heck reaction of aryl halide with methyl acrylate, in which $[PdCl_2(Ph_2PCH_2)_2NMe]$ and $[PdBr_2(Ph_2PCH_2)_2NMe]$ complexes were used as catalysts, can be considered [42]. In this study it was found that $[PdBr_2(Ph_2PCH_2)_2NMe]$ complex is a much more effective catalysts then $[PdCl_2(Ph_2PCH_2)_2NMe]$ complex. When the structures of these two complexes are compared, even though the initial bite angles are almost the same (94.93° for Cl complex and 94.58° for Br complex), Br complex is much more reactive than the Cl complex [42]. So, the superiority of the Br complex on the Cl complex could be attributed to the other parameters for example, the charges on the Pd atoms. The charge on the Pd atom for the Br complex (-0.363) is bigger than that of the Cl complex (-0.313) which may play a role in the binding of the substrate to the M atom. As an attempt to improve on this reaction, the iodine derivatized complex $[PdI_2(Ph_2PCH_2)_2NMe]$, which also have even more charge on the Pd atom than the Br derivative, may function as an even better catalyst considering the longer Pd-I bond lengths it possesses.

The complex $[PdCl_2(Ph_2PCH_2)_2NPh]$ has an interesting structure. As it was noted earlier (page) the two phenyl groups on different P atoms and the phenyl group on the N forms a cage like structure. There is a certain amount of space (about 3.880 Å) between the phenyl group on the N atom and the phenyl groups on the phosphorus atom in which molecules of certain size can fit. In this way, a kind of selectivity can be introduced by the complex $[PdCl_2(Ph_2PCH_2)_2NPh]$ for a specific reaction.

These complexes can be attached easily to a solid support or another molecule via N atom. When we consider the structure of $[PdCl_2(Ph_2PCH_2)_2NPh]$ complex, we can think of it as if it is attached to a solid support whose tip is a phenyl group through N atom. So we can more or less estimate the changes upon attaching it to that kind of solid support. The

attachment of the Ph group on N atom increases only the charge on the Pd atom which may affect the binding of the substrate to the metal atom.

REFERENCES

1. Pignolet, L.H. (ed) *Homogeneous Catalysis with Metal-Phosphine Complexes*, Plenum Press, New York, 1983.
2. Roundhill, R M, *Comprehensive Coordination Chemistry*, Ch.51, Pergamon, Oxford, 1987.
3. Verkade, J.G. and Mosbo, *J 31P NMR Spectroscopy in Stereochemical Analysis*, Verkade, J.G. and L.D. Quin (eds), VCH, pp. 425, Florida, 1987.
4. Hoye, P.A.T., R.D.W. Kemmittt and D.L Law, *Applied Organometallic Chemistry*, Vol. 7, pp. 513-516, 1993.
5. Arya, P., N.V. Rao and J. Singkhonrat, *Journal of Organic Chemistry*, Vol. 65, pp. 1881-1885, 2000.
6. Reetz, M.T. and S.R.Waldvogel, *Angewandte Chemie International Edition*, Vol. 36. No. 8, pp. 865-867, 1997.
7. Urus, S., O. Serindag and M. Digrak, *Heteroatom Chemistry*, Vol. 16, No. 6, pp. 484-491, 2005.
8. Power, P. P., H. Hope, M. Viggiano and B. Moezzi, *Inorganic Chemistry*, Vol. 23, pp. 2550-2552, 1984.
9. Balueva, A.S., R.M. Kuznetsov, I.A. Litvinov, A.T. Gubaidullin, G.N. Nikonov, A.A. Karasik and O.G. Sinyashin, *Russian Chemical Bulletin International Edition*, Vol. 51, No. 1, pp. 151-156.
10. Woolins, J.D., Q. Zhang, G. Hua, P. Bhattacharyya and A.M.Z. Slawin, *European Journal of Inorganic Chemistry*, pp. 2426-2437, 2003.
11. Karasik, A.A., I.O. Georgiev, O.G. Sinyashin and E. Hey-Hawkins, *Polyhedron,* Vol. 19, pp. 1455, 2000.
12. Karasik, A.A., I.O. Georgiev, E.I. Musina, O.G. Sinyashin and J.Heinicke, *Polyhedron*, Vol. 20, pp. 3321, 2001.
13. Hawkins, H.E., A.A. Karasik, R.N. Naumov, R. Sommer and O.G. Sinyashin, *Polyhedron*, Vol. 21, pp. 2251-2256, 2002.
14. Tolman, C.A., *Chemical Reviews*, Vol. 77, No.3, 313-348, 1977.
15. Leeuwen, P.W.N.M., P.C.J. Kamer and J.N.H. Reek, *Pure Applied Chemistry*, Vol. 71, No.8, pp. 1443-1452, 1999.

16. Leeuwen, P.W.N.M., P.C.J. Kamer, J.N.H. Reek and P. Dierkes, *Chemical Reviews*, Vol. 100, pp. 2741-2769, 2000.
17. Hayashi, T., Y. Kawabta, T. Isoyama and I. Ogata, *Bulletin Chemical Society of Japan*, Vol. 54, pp. 3438, 1981.
18. Collman, J. P., L.S. Hegedus, J.R. Norton and R.C. Finke, *Principles and Applications of Organotransition Metal Chemistry*; University Science Books: Mill Valley, Ch. 6, CA, 1987.
19. Yamamoto, A. *Organotransition Metal Chemistry*; Wiley: Ch. 6, New York, 1986.
20. Romeo, R., G. Alibrandi and L.M. Scolaro, *Inorg. Chem.*, Vol. 32, pp. 4688-4694, 1993.
21. Romeo, R., P. Uguagliati and U. Belluco, *J. Mol. Catal.*, Vol. 1, pp. 325-366, 1975/1976.
22. Alibrandi, G., M. Cusumanu, D. Minniti, L.M. Scolaro and R. Romeo, *Inorg. Chem.* Vol. 28, pp. 342-347, 1989.
23. Coussens, B.B., B. Francesco, H. Oevering and R.J. Meier, *Organometallics,* Vol. 17, pp. 795-801, 1998.
24. Jensen, F., *Introduction to Computational Chemistry*, Wiley, New York, 2001.
25. Parr, R. G. and W. Yang, *Density Functional Theory of Atoms and Molecules*, Oxford University Press, New York, 1989.
26. Lee, C., W. Yang and R. G. Parr, "Development of Colle-Salvetti Correlation Energy Formula into a Functional of the Electron Density", *Phys. Rev. B*, Vol. 37, pp. 785-789, 1988.
27. Hay, P. J. and W. R. Wadt, "Ab initio effective core potentials for molecular calculations. Potentials for the transition metal atoms Sc to Hg.", *J. Chem. Phys*. Vol. 82, pp. 270-283, 1985.
28. Wadt, W. R. and P. J. Hay, "Ab initio effective core potentials for molecular calculations. Potentials for main group elements Na to Bi.", *J. Chem. Phys*. Vol.82, pp. 284-298, 1985.
29. Hay, P. J. and W. R. Wadt, "Ab initio effective core potentials for molecular calculations. Potentials for K to Au including the outermost core orbitals", *J. Chem. Phys.* Vol.82, pp. 299-310, 1985.
30. SPARTAN'04 for Windows 1.03, Wavefunction, Inc.18401, Von Karman Ave., 370 Irvine,CA 92715 USA. ©2004 Wavefunction,Inc.

31. Becke, A. D., "Density Functional Thermochemistry. III. The Role of Exact Exchange", *J. Chem. Phys.,* Vol. 98, pp. 5648-5652, 1993.
32. Lee, C., W. Yang and R. G. Parr, "Development of Colle-Salvetti Correlation Energy Formula into a Functional of the Electron Density", *Phys. Rev. B*, Vol. 37, pp. 785-789, 1988.
33. Frisch, M. J., W. Trucks, .B. Schlegel, G.E. Scuseria, M.A. Robb, J.R. Cheeseman, V.G. Zakrewski, J.A. Montgomery, R.E. Stratmann, J.C. Burant, S. Dapprich, J.M. Millam, A.D. Daniels, K.N. Kudin, M.C. Strain, O. Farkas, J. Tomasi, V. Barone, M. Cossi, R. Cammi, B. Mennuci, C. Pomelli, C. Adamo, S. Clifford, J. Ochterski, G.A. Petersson, P.Y. Ayala, Q. Cui, K. Morokuma, D.K. Malick, A.D. Rabuck, K. Raghavachari, J.B. Foresman, J. Cioslowski, J.V. Ortiz, B.B. Stefanov, G. Liu, A. Liashenko, P. Piskorz, A. Komaromi, R. Gompertz , R.L. Martin, D.J. Fox, T. Keith, M.A. Al-laham, J.Y. Peng, A. Nanayakkara, C. Gonzales, M. Challacombe, P. M. W. Gill, B.G. Johnson, W. Chen, M.W. Wong, J.L. Andres, M. Head-Gordon, E.S. Replogle and J.A. Pople, Gaussian, Inc., Pittsburgh PA, 1998.
34. Serindag, O., *The Synthesis of Some Aminobis(methylphosphines) and Their Transition Metal Complexes*, Ph.D. Thesis, University of Leicester, 1993.
35. Suresh, C.H. and N. Koga, *J. phys. Chem. A*, Vol. 105, pp. 5940, 2001.
36. a) Liao, M.S. and W.H.E. Schwarz, *J.Alloys Compounds*, Vol. 246, pp. 2, 1997. b) Acta cryst. B, Vol. 50, pp. 9, 1994.
37. Tripathi, U.M., A. Bauer and H. Schmidbauer, *J.Chem.Soc., Dalton Trans.,* Vol. 17, pp. 2865, 1997.
38. Fujisawa, K., S. Imai and Y. Moro-oka, *Chem.Lett.,* Vol. 27*, pp.* 167, 1998.
39. Fernandez, E. J., J. M. Lopez-de-Luzuriaga, M. Monge, M.A. Rodriguez, O. Crespo, M.C. Gimeno, A. Laguna and P.G. Jones, *Inorg. Chem*., Vol. 37, pp. 6002, 1998.
40. Leznoff, D. B, B.-Y. Xue, R.J. Batchelor, F.W.B. Einstein and B.O. Patrick, *Inorg.Chem*., Vol. 40, pp. 6026, 2001.
41. Bachman, R.E. and D.F. Andretta, *Inorg.Chem*., Vol. 37, pp. 5657, 1998.
42. Keles M., M. Aydin and O. Serindag , *Journal of Organometallic Chemistry*, Vol. 692, pp. 1951–1955, 2007.